THE UNIVERSITY OF MICHIGAN

INDUSTRY PROGRAM OF THE COLLEGE OF ENGINEERING

IRON SILICA SAND INTERFACE REACTIONS

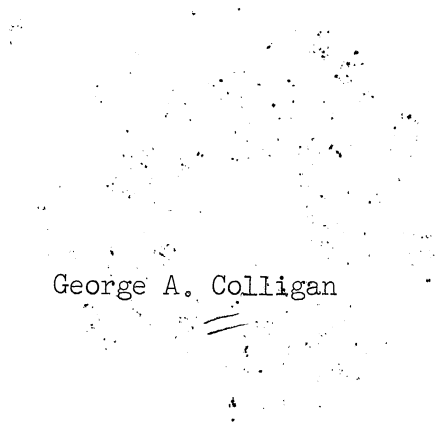

George A. Colligan

A dissertation submitted in partial fulfillment
of the requirements for the degree of
Doctor of Philosophy in the
University of Michigan
1959

October, 1959

IP-390

ensm

UMR6704

Doctoral Committee:

Professor Lawrence H. Van Vlack, Chairman
Assistant Professor Wilbur C. Bigelow
Associate Professor Lee O. Case
Professor Richard A. Flinn
Associate Professor Donald R. Mason
Professor Lewis S. Ramsdell

PREFACE

I wish to express my appreciation to all those who have aided in this investigation and particularly to the following:

Professor Lawrence H. Van Vlack, Chairman of the Doctoral Committee, for his encouragement, suggestions and assistance during the course of this investigation. His unselfish donation of time was invaluable and greatly facilitated this research.

Professors Richard A. Flinn and Lee O. Case, members of the Doctoral Committee, for their advice and critical analyses during this investigation.

Professors Wilbur C. Bigelow, Donald R. Mason, and Lewis S. Ramsdell, members of the Doctoral Committee, for their interest and cooperation.

Mr. Frank B. Drogosz for his invaluable assistance and encouragement during the construction of the high temperature furnace used in these studies.

My fellow graduate students in Metallurgical Engineering for their cooperation, assistance and enlightening discussions.

Mr. Ralph Wells, Mr. Otto Riegger, and Mr. Robert Warrick for their assistance in the experimental phases of this program.

The Industry Program of the College of Engineering for the reproduction of this thesis.

TABLE OF CONTENTS

	Page
PREFACE	iii
LIST OF TABLES	v
LIST OF FIGURES	vi
INTRODUCTION	1
REVIEW OF LITERATURE	3
Literature Pertaining to Penetration and Interface Reaction	3
Literature Pertaining to Phase Equilibrium	7
SUMMARY OF LITERATURE	9
EXPERIMENTAL PROCEDURE	10
Equilibrium Studies	10
Test Casting Evaluation	19
RESULTS	21
Iron-Silica Equilibria	21
Effect of Manganese Additions	24
Test Casting Evaluation	27
DISCUSSION OF RESULTS	30
Discussion of Laboratory Equilibration Results	30
Discussion of Engineering Significance	33
CONCLUSIONS	38
APPENDIX I. Chemical Compositions of Mineral Phases	73
APPENDIX II. High Temperature Furnace Construction	74
APPENDIX III. Calculation of Univariant Equilibrium Solid Metal, Liquid Metal, Silica, Gas	76
BIBLIOGRAPHY	78

LIST OF TABLES

No.		Page
I	Chemical Analysis of Vacuum Melted Iron	40
II	Summary of Equilibration Experiments	41
III	Sand Mixtures for Test Castings	42
IV	Summary of Test Castings	43
V	Calculated Univariant Equilibrium Solid Metal, Liquid Metal, Silica, Gas	44

LIST OF FIGURES

No.		Page
1	Equilibrium diagram after Darken.	45
2	Shell mold for test step-casting.	46
3	Surface condition of sample A-55.	47
4	Surface condition of sample A-49.	47
5	Microstructure of sample A-55.	48
6	Microstructure of sample A-49.	48
7	Microstructure of sample B-17.	49
8	Microstructure of sample B-21.	49
9	Microstructure of sample B-4.	50
10	Microstructure of sample B-3.	50
11	Microstructure of sample C-9.	51
12	Microstructure of sample C-6.	51
13	Microstructure of sample C-8.	52
14	Microstructure of sample C-7.	52
15	Microstructure of sample D-10.	53
16	Microstructure of sample D-4.	53
17	Microstructure of sample D-7.	54
18	Penetration of iron in sample D-7.	54
19	Surface condition of sample D-11.	55
20	Microstructure of sample D-11.	55

LIST OF FIGURES (Continued)

No.		Page
21	Microstructure of sample A-43.	56
22	Microstructure of sample A-47.	56
23	Microstructure of sample A-58.	57
24	Microstructure of sample A-57.	57
25	Microstructure of sample B-19.	58
26	Microstructure of sample B-15.	58
27	Microstructure of sample C-15.	59
28	Microstructure of sample C-10.	59
29	Microstructure of sample D-12.	60
30	Microstructure of sample A-54.	60
31	Microstructure of sample B-11.	61
32	Microstructure of sample C-16.	61
33	Microstructure of sample D-13.	62
34	Microstructure of sample C-11.	62
35	Microstructure of sample D-9.	63
36	Photograph of test step-casting, E-1.	64
37	Photograph of test step-casting, E-2.	64
38	Photograph of test step-casting, E-3.	65
39	Photograph of test step-casting, E-4.	65
40	Microstructure of sintered layer from test step-casting, E-1.	66
41	Microstructure of sintered layer from test step-casting, E-2.	66
42	Microstructure of sintered layer from test step-casting, E-3.	67

LIST OF FIGURES (Concluded)

No.		Page
43	Microstructure of sintered layer from test step-casting, E-4.	67
44	Microstructure of sintered layer from greensand cope of test step-casting, E-8.	68
45	Microstructure of sintered layer from shell sand drag of test step-casting, E-8.	68
46	Equilibrium diagram from Darken modified to include present experimental results.	69
47	Equilibrium diagram from Darken modified to include the effect of manganese additions.	70
48	Detailed drawings of high-temperature furnace.	71
49	Photograph of high-temperature-furnace control panel.	72
50	Photograph of high-temperature-furnace shell and control panel.	72

INTRODUCTION

The objective of this research was to study the reactions that take place at the interface between iron and silica with varying atmospheres over the range of temperatures experienced in producing an iron-base cast alloy. In order to prevent or minimize these reactions a thorough understanding of the nature of the reactions is necessary. This understanding can best be accomplished by determining the equilibrium situation between iron, silicon, oxygen and carbon in the presence of a strong excess of silica. Once the basic equilibrium situation is known the effects of additional variables such as manganese may be studied.

Mold-metal interface reaction has historically been a serious problem in the field of cast metals. This interface reaction between metal and mold material is the cause of surface roughness, dimensional inaccuracy, metal penetration and "fused sand." The solution to this problem has been approached as unique for each individual casting, mold material and alloy. Considerable success has been accomplished by varying mold washes, gating systems, sand additives and pouring temperatures. Each solution, however, was designed for a single set of experimental conditions.

The determination of equilibrium data for the system iron-silicon-oxygen-carbon combined with the evaluation of manganese additions to the iron will aid in understanding the nature of the interface reaction. In

addition, these results combined with test casting results should explain the mechanism of "sand fusion" and metal penetration as well as the procedures to follow in order to minimize these problems.

REVIEW OF LITERATURE

The review of the literature can best be considered in two categories:

1. Penetration and interface reaction
2. Phase equilibria

Literature Pertaining to Penetration and Interface Reaction

A considerable amount of work has been done in this field of penetration and is summarized by Murton and Gertsman.[1]

Caine's[2] experiments consisted of immersing sand specimens in liquid metal. Penetration was found to be a function of sand geometry, i.e., pore size. The effect of chemical reaction was not considered. Dietert[3] discussed the effects of mold atmosphere variation. His investigation was made on low carbon steel pins imbedded in silica sand. The sample was heated in a dilatometer and the resultant metal-sand interface observed. The atmosphere in the furnace was controlled by use of gases (oxygen, nitrogen and CO_2) and by additions of various compounds to the sand mixture. The resultant "oxide penetration" was greatly decreased by neutral or reducing atmosphere in the furnace. It was observed that the liquid oxide formed at the interface was "absorbed" into the silica sand very rapidly. The reaction products were not positively identified

and repeated reference was made to a "fluid iron silicate" of three possible stoichiometric forms. This research was the first significant attempt to study the effect of atmosphere on mold-metal interface reaction.

Savage and Taylor[4] studied the effect of atmosphere on interface reaction products for 1040 steel and Armco iron pins imbedded in silica sand and heated in an induction field. The results of x-ray diffraction study showed the presence of fayalite* in the sinter layer with an air atmosphere. This fayalite zone could be eliminated by use of a nitrogen or hydrogen atmosphere during melting. The effect of bentonite additions to the sand was to favor the formation of a reaction product at the metal-mold interface. Alloy additions (C, Mn and Si) to the iron were felt to have reduced the tendency for interface reaction since they would oxidize preferentially to the iron. No direct methods of observation of the reaction zone were used and therefore no study of the nature of this zone was possible. The importance of atmosphere control was plainly demonstrated, but no effort was made to consider surface tension effects.

Giller[5] found that with rapid cooling of a silicate melt a glass was formed. Slow cooling of the iron silicate melt resulted in crystallization of fayalite.

Hoar and Atterton[6] determined that the pressure necessary to initiate penetration was a function of the surface tension of the metal. By using a pressure differential through a sand platen they found that tin, whose surface energy was 500 dynes/cm, required a pressure of 15 cm of

*The chemical compositions of all mineral phases are tabulated in Appendix I.

Hg to initiate penetration. Using the same technique copper, whose surface energy was 1000 dynes/cm, required a pressure differential of 30 cm of Hg to cause penetration. In the case of pure iron Atterton[7] reports a surface tension of 1550 dynes/cm and discusses the effect of wetting or non-wetting on interface reaction and penetration. Armco iron in contact with a silica plaque was melted in (a) vacuum and (b) air atmosphere. Observations of the resulting sessile drops indicated large contact angles ($\theta > 90°$) in both cases. The iron melted in air, however, produced an iron oxide liquid which wetted both the iron and the silica plaque. The effects of oxygen pressure and carbon content were not clearly explained.

Several investigators have shown that the role of carbon and oxygen as well as other alloying elements is quite important on iron surface tension and iron-refractory oxide interfacial energy.

Kozakevich, Chatel and Sage[8] reported the effect of carbon on iron surface tension in the following expression:

$$\sigma_{iron} = 1600 - 100 \text{ (wt \% C) dynes/cm for wt \% C} = 0.1 \rightarrow 5.0\% \ .$$

This result would indicate a tendency for carbon to increase the ease of penetration.

Halden and Kingery[9] studied the effect of sulfur, oxygen, nitrogen, and carbon on iron surface tension and Fe-Al_2O_3 interfacial energy. They demonstrated that carbon variation from 0.027 → 3.39% has a very slight effect on iron surface tension (1717 → 1708 dynes/cm). The same carbon variation actually increased the contact angle from 104.5 to 111.6° and

raised the Fe-Al_2O_3 interfacial energy from 1365 to 1563 erg/cm^2. Oxygen, however, drastically reduced the surface tension, contact angle and interfacial energy.

Petersson[10] studied the problem of penetration by using an immersion test. His experiments considered both the geometry and chemical reaction aspects of the problem. Increasing carbon and aluminum content in the metal reduced penetration, and addition of metallic aluminum to the molding material, also, reduced penetration. Petersson concluded that penetration was largely a mechanical problem and that the role of chemical reaction was greatly exaggerated. It was noted, however, that anything that caused a reduction in the metal surface tension (i.e., improved metal-silica wetting) or increased the effective pore size in the mold wall would greatly favor penetration.

Emmons and Bach[11] studied the problem of steel penetration in silica sand. Microscopic observation of the penetrated sand indicated the presence of some fayalite and cristobalite. Gas samples were removed from the molds after pouring and analyzed. The gas consisted predominantly of CO, H_2, CO_2, O_2 and H_2O. The results of this work led to a hypothesis of penetration of iron in the form of a metastable iron carbonyl in the temperature range of 1000°C. Upon decomposition the gas deposits pure iron in the sand interstices at some distance from the original interface. The fact that CO and H_2 comprise 50-75% of the gas evolved is an essential condition to permit the iron carbonyl Fe $(CO)_5$ formation.

In addition to this phase of their study, some qualitative inter-

facial energy experiments were performed. Low carbon steel cubes were melted on fused silica and silica sand in atmospheres of nitrogen, wet and dry hydrogen, carbon monoxide, carbon dioxide, and air. Under reducing conditions high non-wetting contact angles prevailed. Under oxidizing conditions a liquid iron oxide formed and the "liquid steel wets the silica."

Literature Pertaining to Phase Equilibrium

Since it is clearly established that interface reaction is basically the attempt of the multicomponent system Fe-Si-O-C and other alloying elements to equilibrate under existing conditions of temperature, a fundamental knowledge of the various phase equilibria is necessary to understand the reaction.

The phase equilibria in the Fe-Si-O system have been investigated by Bowen and Schairer[12] and Muan.[13] This work was mainly concerned with liquidus surface determination. Koerber and Oelsen[14] studied the quaternary system Fe-Si-O-Mn by heating admixtures of iron and slag (FeO-MnO) in silica sand crucibles. After equilibration in air the products were chemically analyzed. The equilibrium partition of Si and Mn between metal and slag (SiO_2 and MnO) was determined in this manner.

Darken and Gurry[15] studied the Fe-O system and the thermodynamics of the liquid oxides and other phases.

The most important research was performed by Darken[16] and was concerned with the melting points of iron oxide on solid silica. Prior to

this time very little work had been done on the effect of gas composition on the melting temperatures of the various iron oxides. The effect of gas composition and temperature on two univariant equilibria was examined by equilibrating a silica rod coated with hematite in a controlled atmosphere, gradiant furnace.

The experimental results of this study were combined with previous experimental and thermodynamic data to construct an equilibrium diagram. This diagram, Figure 1, plots the phase equilibria as a function of temperature and log p_{CO_2}/p_{CO}. The log ratio of p_{CO_2} and p_{CO} may be converted to partial pressure of oxygen by using the known equilibrium constant for the reaction $CO + 1/2\ O_2 \rightarrow CO_2$. In this diagram the following three univariant equilibria are plotted from experimental and thermodynamic data:

(a) metal, silica, fayalite, gas

(b) fayalite, silica, melt, gas

(c) magnetite, silica, melt, gas

The equilibria metal, silica, melt, gas is "estimated roughly in the following manner: Iron melts in contact with its molten oxide at about 1525°, at which temperature log $p_{CO_2}/p_{CO} = -0.68$; it is estimated that the activity of ferrous oxide in the oxide phase in equilibrium with iron is depressed by saturation with silica to about one-third, thus at 1525° the value of log p_{CO_2}/p_{CO} is $-0.68 - \log 3 = -1.16$."

This assumption of one-third the oxygen activity in a silica saturated slag is based on earlier work of Koerber and Oelsen.[14] This univariant equilibrium curve is then approximately determined by this point and the invariant quintuple point, fayalite, metal, silica, melt and gas.

SUMMARY OF LITERATURE

From the review of the literature and the phase equilibria studies of the system it seems that there are two basic mechanisms involved in interface reaction and penetration.

Mechanical Factors

Penetration may be affected by pressure, bulk density of refractory material at the interface and strength of the refractory mold material.

Chemical Factors

Penetration and reaction may be affected by metal composition, gas composition and temperature.

In view of the contradictory results and the lack of fundamental information on the chemical factors involved in penetration and reaction, it seemed a fruitful area for research.

EXPERIMENTAL PROCEDURE

To develop a thorough understanding of the problem of iron-silica interface reaction, the basic equilibrium must be studied. In addition the actual conditions experienced at the mold-metal interface during casting operations should be evaluated. The procedure section of this research is considered in the following sequence: 1) equilibrium studies and 2) test casting evaluation.

Equilibrium Studies

The necessary phase equilibria investigations were performed in a controlled atmosphere, high temperature, molybdenum resistance furnace. The details of the construction of this furnace are included in Appendix II and Figures 48, 49 and 50. These experiments were first outlined by a phase rule analysis of the system which follows.

After the phase rule analysis a detailed description of the procedures is presented in the following sequence, preparation of experimental materials, temperature control, gas composition control, equilibration technique and phase identification.

Phase Rule Analysis

The study of this Fe-Si-O-C system is greatly facilitated by maintaining a constant gas pressure slightly greater than one atmosphere.

The phase rule is then reduced to

$$P + V = C + 1$$

where P = the number of phases

V = variance or degrees of freedom

C = the number of components

For the four component system Fe-Si-O-C, the dashed line in Figure 1, represents four phase equilibrium according to Darken. To understand clearly the nature of this system, however, we should evaluate it more rigorously as outlined by Case[17]:

N = the number of individual chemical substances

G = the number of independent distributions of the same chemical individual

E = the number of additional relations among the concentration variables, i.e., mass action equilibria

U = the number of variables, i.e., pressure, temperature and one less concentration variable than the number of individuals in each phase

$$C = N - E \qquad V = C + 2 - P$$

$$V = U - G - E$$

Point 2 calculated by Darken is actually an invariant quintuple point at which the five phases—gas, silica, solid metal, liquid metal and liquid silicate melt—are in equilibrium. Using the phase rule we find a unique point at constant pressure. From this point there will be four, univariant four phase equilibria radiating:

(a) solid metal, liquid metal, silica, gas

(b) solid metal, liquid silicate melt, silica, gas

(c) liquid metal, liquid silicate melt, silica, gas

(d) liquid metal, liquid silicate melt, solid metal, gas

Since our interest is limited to conditions with a strong excess of silica equilibria a, b and c are of practical significance. The dashed line connecting points 1 and 2 in Figure 1 is Darken's predicted position of equilibrium b. This univariant boundary and the adjacent bivariant fields are analyzed as follows:

(a) Equilibrium under oxidizing conditions.—

System: $CO_{2(g)}$, $CO_{(g)}$; $SiO_{2(s)}$; $2FeO \cdot SiO_{2(\ell)}$

$P = 3$ gas, solid, liquid

$N = 4$ CO_2, CO, SiO_2, FeO

$U_p = 3$ 2 - 1 = 1 (gas) 2 - 1 = 1 (liquid) plus 1 (temperature)

$G = 1$ $SiO_{2(s)} \rightarrow SiO_{2(\ell)}$

$E = 0$

$C = N - E = 4$ $\qquad V_p = C + 1 - P$

$V_p = U_p - G - E$ $\qquad V_p = 2$

$V_p = 2$

The phase rule variables in this system are temperature, gas composition and liquid composition. All composition variables include the mole fraction of each chemical individual in the particular phase under consideration. By controlling the temperature and gas composition we fix the system in the experimental work performed.

(b) Equilibrium under reducing conditions.—

System: $CO_{2(g)}$, $CO_{(g)}$; $SiO_{2(s)}$; C in $Fe_{(s)}$

P = 3 gas, 2 solids

N = 5 CO_2, CO, SiO_2, C, Fe

U_p = 3 2 - 1 = 1 (gas), 2 - 1 = 1 (solid), plus 1 (temperature)

G = 0

E = 1 $CO_2 + C \rightarrow 2\,CO$

$C = N - E = 4$ $V_p = C + 1 - P = 2$

$V_p = U_p - G - E = 2$

The phase rule variables in this system are temperature, gas composition and solid iron composition. By controlling the temperature and gas composition we fix the system in the experimental work performed.

(c) Equilibrium at phase field boundary.—

System: $CO_{2(g)}$, $CO_{(g)}$; $SiO_{2(s)}$; C in $Fe_{(s)}$; $2FeO \cdot SiO_{2(\ell)}$

P = 4 gas, 2 solids, liquid

N = 6 CO_2, CO, SiO_2, C, Fe, FeO

U_p = 4 2 - 1 = 1 (gas), 2 - 1 = 1 (solid Fe),

2 - 1 = 1 (liquid $2FeO \cdot SiO_2$), plus 1 (temperature)

G = 1 $SiO_{2(s)} \rightarrow SiO_{2(\ell)}$

E = 2 $CO_2 + C \rightarrow 2CO$

$Fe + CO_2 \rightarrow FeO + CO$

$C = N - E = 4$ $V_p = C + 1 - P = 1$

$V_p = U_p - G - E = 1$

The phase rule variables in this system are temperature, gas composition, solid iron solution composition and the liquid silicate melt composition. By controlling the temperature we fix this univariant equilibria.

Equilibria a and c analyzed in the same manner yield univariant curves at constant pressure. All three of these curves must radiate from the same invariant quintuple point. The combination of experimental investigation and available thermodynamic data should permit the determination of the position of these univariant curves, the invariant quintuple point and the effect of temperature, atmosphere and manganese content on interface reaction and penetration.

Preparation of Experimental Materials

Cold rolled vacuum melted iron discs (Table I) were cut from 1/2-inch-diameter round stock, cleaned in hydrochloric acid, rinsed in water and then acetone before use. The iron-manganese alloys were produced as two master heats. Vacuum melted iron and manganese metal were melted in an inert atmosphere induction furnace to produce the two heats of 1.0% and 9.85% manganese. These master ingots were machined to produce small chips for experimental use. The chips were cleaned in the same manner as the iron discs.

Temperature Control

Temperature control was accomplished by calibrating the furnace controller with a separate platinum-platinum 10% rhodium thermocouple. The furnace controller is activated by a radiation pyrometer which sights on

a closed end mullite tube in contact with the center molybdenum resistance coil.

For each temperature investigated a vitreous silica crucible containing quartz sand was placed on the specimen plaque. The platinum thermocouple enclosed in an impermeable recrystallized alumina protection tube was placed in the quartz sand. The temperature was then calibrated with air and with a CO_2/CO atmosphere in the muffle. The thermocouple was calibrated against the melting point of pure iron 1539°C (2802°F). The major variation in temperature was due to line voltage variation in the building which resulted in an accuracy of ± 2°C. Since the controller pyrometer uses the radiation in a closed end tube as the source of emf for temperature measurement and control there is no contamination of thermocouples from the muffle atmosphere during experimental runs.

Gas Composition Control

"Bone Dry Grade" carbon dioxide and "C.P." carbon monoxide were used to vary the oxygen potential in the furnace muffle. These gases were purified by passing over calcium chips and copper gauze at 600°C (1112°F) and dried with calcium sulfate and activated alumina.

Flowrator flow meters were calibrated for CO and CO_2 gases at ambient temperature and 10 psig pressure. These flow meters were used to obtain preliminary mixing ratios. Final adjustment of the gas ratios was made by adjustments based on chemical analysis of samples from the inlet line. Standard caustic solution was used to absorb the CO_2, the remaining

CO was removed by oxidizing it to CO_2 in a copper oxide furnace and adsorbing this in the caustic. Finally any unoxidized CO was removed with cuprous chloride. The gas composition was analyzed before, during and after experimental runs. The resultant control yielded accuracy of ± .2% on the analysis of either component of the mixture. This accuracy of analysis was verified by analyzing known mixtures of gas from cylinders previously analyzed with the mass spectrograph.

Equilibration Technique

The quartz sand was placed in a vitreous silica crucible and weighed. The metallic charge was then added to the crucible, forced beneath the surface of the quartz to allow intimate contact between the iron and quartz, and weighed. The crucible was then introduced into the top of the furnace and suspended in the cold end on platinum wire for thirty minutes. The gas atmosphere in the furnace outlet line returned to the inlet line analysis in fifteen minutes. The crucible was then lowered into position in the recessed surface of the alumina plaque in the hot zone. At the completion of the run the crucible was cooled in the furnace atmosphere by raising it into the cold end of the furnace for five minutes. A summary of the equilibration experiments is contained in Table II.

To eliminate the problem of thermal diffusion in the furnace atmosphere low flow rates were avoided and the gas was introduced at the bottom of the furnace as outlined by Darken.[15]

Univariant Equilibria

In order to determinine accurately the position of the boundary between the gas, silica, melt and gas, silica, metal fields it seemed desirable to approach the boundary from two directions. The iron-silica charge was used to determine the appearance of the first interface reaction, i.e., silicate melt formation. Completely oxidized melts saturated with silica at the temperature under investigation were used to approach the boundary from the gas, silica, melt field. In this case polished sections were used to determine the atmosphere which reduced the iron silicate liquid and precipitated iron prior to cooling.

Four temperatures were investigated in this research: 1250°C (2282°F) 1400°C (2552°F), 1500°C (2732°F) and 1550°C (2822°F). This temperature range covers solid iron-silica reactions as well as liquid iron-silica reactions. These temperatures were chosen since the reactions are just as serious below the melting point of iron as above it.

At each temperature the iron-silica charge was used first to determine the approximate atmosphere necessary to prevent silicate melt formation. The final runs used couples of iron-silica and silicate melt-silica charges to bracket the boundary. Following each experimental run the iron disc was examined visually for evidence of silicate melt formation. At the low temperatures, i.e., below the melting point of iron, the silica grains exhibit no adhesion to the iron in the absence of a silicate melt. Under conditions sufficiently oxidizing to allow the formation of a silicate melt, the silica could not be removed from the iron.

The individual sand grains fracture leaving the iron disc coated with silica grains imbedded in a silicate melt.

Above the melting point of the iron, i.e., 1550°C (2822°F), the presence or absence of a silicate melt could be observed macroscopically, and the necessary variation in atmosphere made to determine the phase field boundary position. All visual inspection was verified by optical microscopy techniques.

Iron-Manganese Alloys

The effect of manganese additions of 1% and 9.85% was studied in exactly the same manner as the pure iron-silica interface reactions. The charge material used was iron-manganese chips instead of iron discs. The equilibration technique was identical to that outlined previously. Iron-manganese-silica charges as well as silicate-silica charges were used to study the effect of manganese additions. The appearance of a silicate melt and the reduction of iron from a silicate melt were observed both macroscopically and microscopically.

Phase Identification

The charges after exposure at elevated temperature and controlled atmosphere were cooled in the atmosphere under study and removed from the furnace. In some cases the reaction couple was photographed to preserve its macroscopic appearance. To allow high magnification observation the samples were first impregnated in a vacuum with a thermosetting resin to reduce their friability. The impregnated sample was then mounted in

a thermoplastic resin and polished for reflected light microscopic observation. The polished samples were studied to permit phase identification of the resultant reaction products. These phases had been identified by optical and x-ray diffraction techniques in previous studies.[18,19]

Test Casting Evaluation

The actual atmospheres obtained in a sand mold during casting operations are of great concern. In order to correlate the equilibrium data with actual practice the following experiments were performed. The effect of manganese additions and atmosphere on interface reaction was qualitatively evaluated on test castings in the following manner. Identical step castings were produced in green sand molds, shell molds, Figure 2, and molds containing a shell sand drag and greensand cope. The sand mixtures are summarized in Table III. By using a greensand mixture an oxidizing condition is produced at the metal-mold interface, Emmons and Bach.[11] The resin-bonded shell mold produces strongly reducing conditions as determined by Van Vlack, Wells and Pierce.[20]

Melting Procedure

Cold rolled AISI 1018 bar stock was melted in a high frequency induction furnace. After melt down a small silicon addition was made to deoxidize the melt and allow recarbonization to the desired level. This level was calculated from experimental equilibrium data at 1550°C (2822°F) under controlled atmosphere. The chemical composition of these castings

is recorded in Table IV, which contains a complete summary of experimental data.

The manganese additions were made to the furnace after pouring the simple iron-carbon alloy.

Casting Procedure

Compositions of 0.23%, 0.75% and 4.40% manganese were each initially cast in a greensand mold and a shell mold to determine the effect of atmosphere and manganese content on interface reaction.

In order to eliminate the problem of pouring temperature variation, duplex molds were poured with 0.50% and 8.60% manganese. These molds each contained a shell sand drag and a greensand cope. In this way a measure of the effect of atmosphere at the interface on reaction can be determined in one mold. All castings were poured from small ladles after tapping the metal from the furnace.

Interface Reaction Evaluation

All castings were observed visually after cooling and in some cases photographed to provide a permanent record. The surface sinter layer was carefully removed from the castings for microscopic examination. Samples of appropriate sintered layer specimens were vacuum impregnated with thermosetting resin, mounted in thermoplastic resin and polished for high magnification observation.

RESULTS

The detailed results of this investigation are presented in the following major categories: (1) iron-silica equilibria, (2) effect of manganese additions, (3) test casting evaluation.

Iron-Silica Equilibria

This section of the results will be considered in the same manner outlined in the phase rule analysis section of the experimental procedure. Each of the three univariant four phase equilibria that are of interest will be considered individually.

Solid Metal, Liquid Silicate Melt, Silica, Gas

The results of iron-silica and silicate-silica charges at 1250°C (2282°F) place the metal-silicate melt boundary between 11.4% CO_2 and 12.3% CO_2.* Figure 3 is a 4.5X photograph of the iron charge after exposure to the 11.4% CO_2 atmosphere. There is no evidence of reaction. The grain size of the iron is revealed by heat tinting on removal from the furnace atmosphere. Figure 4 is a 4.5X photograph of the iron charge after exposure to the 12.3% CO_2 atmosphere. There is extensive sand adherence and loss of detail on the edge of the sample. Figures 5 and 6 are 500X photomicrographs of these same samples indicating reducing con-

*All gas mixtures contain only CO_2 and CO. For simplicity only the % CO_2 is recorded in the body of this report. The % CO in all cases is (100% - % CO_2).

ditions (5), and oxidizing conditions (6).

The results of iron-silica and silicate-silica charges at 1400°C (2552°F) place the metal-silicate melt boundary between 9.2% CO and 9.9% CO_2. Figures 7 and 8 illustrate the appearance of the silicate-silica charge after exposure to reducing, 9.2% CO_2, and oxidizing, 11.5% CO_2 atmospheres. Under reducing conditions large spherical particles of iron are reduced from the iron silicate melt, Figure 7. Under oxidizing conditions, Figure 8, only very small euhedral crystals of iron precipitate on cooling through the iron stable field. Figures 9 and 10 show the iron silica charges at 500X after oxidizing conditions 9.9% CO_2 and after reducing conditions at 7.6% CO_2. Under oxidizing conditions there is extensive formation of an iron silicate melt. With a reducing atmosphere there is no adhering silica or silicate melt on the metallic surface.

At the final temperature of 1500°C (2732°F) the boundary falls between 5.0% CO_2 and 5.5% CO_2. Figure 11 is a 500X photomicrograph of the iron-silica charge under reducing atmosphere, 5.0% CO_2; there is no reaction at the iron-silica interface and therefore there is no silicate melt formed. Figure 12 is a 500X photomicrograph of the iron-silica charge under an oxidizing atmosphere, 5.5% CO_2. The reaction zone containing the silicate melt and cristobalite precipitate is quite evident. Figure 13 is a 500X photomicrograph of the silicate-silica charge exposed to the reducing, 5.0% CO_2 atmosphere. The iron reduced from the silicate melt is quite extensive. Figure 14 is the 500X photomicrograph of the silicate-silica charge after exposure to an oxidizing atmosphere, 5.5% CO_2. There is very slight precipitation of iron from the silicate melt on cooling.

These three experimentally determined points together with the data of Darken establish the position of the univariant equilibrium, solid metal, liquid silicate melt, silica, gas.

Solid Metal, Liquid Metal, Silica, Gas

This univariant equilibria can be approximated by calculation from the well established thermodynamic data available for the reaction:

$$CO_2 + \underline{C} \longrightarrow 2\,CO \quad .$$

Since the solubility of solid silica in liquid and solid iron under reducing conditions is extremely low it will have little effect on the solubility of carbon in iron. Therefore, for a given atmosphere, p_{CO_2}/p_{CO}, and with the calculated equilibrium constant, the equilibrium weight percent carbon dissolved in the iron may be determined. Once the carbon content of the iron is calculated the liquidus temperature may be found on the iron-carbon equilibrium diagram. By calculating this equilibrium carbon content for three different values of p_{CO_2}/p_{CO} the univariant curve may be approximated. A sample calculation is included in Appendix III and the results of these calculations are contained in Table V.

Liquid Metal, Liquid Silicate Melt, Silica, Gas

The intersection of the two univariant equilibria (a) and (b) will take place at the invariant quintuple point. This quintuple point will establish one point on the univariant curve liquid metal, liquid silicate melt, silica, gas.

In addition to these data, experimental results at 1550°C (2822°F)

indicate that the boundary falls between 3.3% CO_2 and 3.9% CO_2. Figures 15 and 16 present the results of the silicate-silica charge under reducing conditions, 3.3% CO_2, and under oxidizing conditions, 4.98% CO_2. The extensive reduction of the silicate melt is evident in Figure 15.

Figure 17 is a 500X section through the interface area of the iron-silica charge after exposure to an atmosphere of 3.9% CO_2. The silicate melt which is the result of interface reaction is quite evident. Figure 18 contains the same specimen at a lower magnification, 25X. The silica grains are completely surrounded by iron due to the extensive reaction at the interface. Figure 19 is a 12X photograph of the surface of the iron-silica charge after exposure to a 3.3% CO_2 atmosphere. There has been no reaction and the silica grains can be easily removed from the depressions in the iron disc. Figure 20 is a 500X photomicrograph of the same sample which exhibits no evidence of liquid silicate melt.

Prior experimental work[18] established that this same system exhibited reducing conditions at 1565°C (2849°F) if the atmosphere was 2.7% CO_2. When all of these data are combined the location of this univariant equilibrium curve is clearly indicated over the temperature range that is critical in cast metals practice.

Effect of Manganese Additions

In general the phase rule indicates that as an additional component is added to a system an additional degree of freedom or variance will result. Therefore, as manganese is added, each of the univariant curves in

the simple iron system will become a bivariant field and will remain so until a new phase appears or a component is removed from the system. In the case of this investigation two levels of manganese additions were made to the iron, 1% and 9.85% by weight.

1% Manganese Alloy

At 1250°C (2282°F) the 1% manganese alloy exhibits reaction until the atmosphere is 10.0% CO_2. Figures 21 and 22 show the results of iron-manganese-silica charges under oxidizing, 10.5% CO_2, and reducing, 10.0% CO_2, atmospheres. The silicate melt formation is quite evident in Figure 21. There is no evidence of reaction in Figure 22.

Figures 23 and 24 contain the results of the iron-manganese-silicate charge samples after exposure to reducing, 9.2% CO_2, and oxidizing, 10.6% CO_2, atmospheres. Under reducing conditions extensive iron-manganese reduction from the silicate melt is experienced, while under oxidizing conditions only small euhedral iron-manganese crystals precipitate on cooling.

At 1400°C (2552°F) there is a silicate melt formed even in a 0.2% CO_2 atmosphere, Figure 25. The iron-manganese alloy is unstable until the atmosphere reaches 7.5% CO_2. Figure 26 is a 500X photomicrograph of the iron-manganese-silicate charge after exposure to the reducing atmosphere, 7.5% CO_2. There is extensive reduction of the silicate melt.

At 1500°C (2732°F) there is extensive reaction even under the most reducing conditions. Figure 27 shows the iron-manganese-silica charge after exposure to 0.2% CO_2 atmosphere; there is extensive silicate melt formed. Figure 28 is a 500X photomicrograph of the iron-manganese-sili-

cate charge under reducing conditions, 4.9% CO_2; considerable iron-manganese alloy has been reduced from the melt.

At 1550°C (2822°F) there is, also, extensive silicate melt formation with an atmosphere of 0.2% CO_2. Figure 29 is a 500X photomicrograph of the iron-manganese-silica charge after exposure to this atmosphere, the silicate melt formation is complete.

9.85% Manganese Alloy

The alloy of 9.85% manganese exhibited extensive silicate melt formation at all temperatures investigated even under the most reducing atmosphere, 0.2% CO_2. Figures 30, 31, 32, and 33 are 500X photomicrographs of the iron-manganese-silica charges after exposure to this atmosphere at 1250°C (2282°F), 1400°C (2552°F), 1500°C (2732°F), and 1550°C (2822°F), respectively. In all cases the presence of a silicate melt is very obvious. In addition, Figures 30, and 31 contain clear evidence of the formation of MnO at and below the surface of the iron-manganese alloys. At temperatures above the melting point, 1500°C (2732°F), there is no sub-scale present.

Iron-manganese-silicate charges for the 9.85% manganese alloy yielded results similar to the 1% manganese alloy. At 1250°C (2282°F) the iron-manganese alloy and silicate melt coexist over the range of atmospheres 10.0% CO_2 to 0.2% CO_2. At 1400°C (2552°F) these two phases coexist from 7.5% CO_2 to 0.2% CO_2. At 1500°C (2732°F) and 1550°C (2822°F) they coexist over the ranges 4.9% CO_2 to 0.2% CO_2 and 3.05% CO_2 to 0.2% CO_2, respectively. Figures 34 and 35 are 500X photomicrographs of the iron-manganese-

silicate charges after exposure to 1500°C (2732°F), 4.9% CO_2, and 1550°C (2822°F), 3.05% CO_2 conditions. In each case the large iron-manganese spheres have been reduced from the silicate melt, and are typical of these experimental results.

Test Casting Evaluation

The results of this qualitative phase of the investigation may best be considered under the following categories:

(a) macroscale evaluation, and

(b) microscopic evaluation of interface reaction.

Macroscale Evaluation

The first series of step castings was poured at three different manganese contents into greensand molds and shell molds. The details of the analysis, mold materials and pouring temperatures are recorded in Table IV.

In general, the difference between greensand and shell sand was very obvious at all levels of manganese content. The oxidizing nature of the greensand mold produced extreme interface reaction, which resulted in poor surface finish, some metal penetration and extensive fusion of the silica at the interface. The reducing nature of the shell sand mold permitted very little interface reaction. The surfaces were smooth, free of metal penetration and exhibited very slight silica fusion. Figure 36 is a photograph of the 0.19% manganese alloy poured in a greensand mold. The heavy sintered layer and very poor surface finish is quite obvious. Figure 37 is a photograph of the same alloy poured in a shell mold. There

is very slight interface reaction and almost no sintered layer, i.e., fused zone of reaction products. The surface finish is smooth and the detail is far superior to the greensand casting in spite of a lower pouring temperature.

Figure 38 is a photograph of the 4.10% manganese alloy poured in a greensand mold. The extensive interface reaction has produced a very heavy sintered layer and extensive silica fusion. Figure 39 is a photograph of the 4.40% manganese alloy poured in a shell mold. The casting exhibits good surface finish, some light reaction and silica fusion. It is interesting to note the superior detail and fluidity in the shell molded casting poured at the lower temperature.

A second set of two castings was produced to eliminate the problem of pouring temperature variation. These molds consisted of a shell sand drag and a greensand cope. The first casting contained 0.50% manganese and exhibited a heavy sintered layer at the greensand interface and very light reaction at the shell sand interface. The second casting was an 8.60% manganese alloy. The greensand interface of this casting was very rough and contained a heavy sintered layer. The shell sand interface was smooth with very slight reaction and no heavy adhering sintered layer.

Microscopic Evaluation of Interface Reaction

Microscopic examination of the sintered layer removed from the experimental castings yielded very interesting results. Figure 40 contains the reaction products from the sintered layer of the 0.19% manganese alloy cast in a greensand mold. There is extensive evidence of the formation

of a liquid silicate melt at high temperature. This melt has essentially crystallized to fayalite on cooling. In addition to the quartz and cristobalite the specimen contains a great deal of magnetite, the small skeletal crystals.

Figure 41 is a photomicrograph of the sintered layer from the 0.23% manganese alloy cast in a shell mold. There is a small amount of silicate melt from the reaction at elevated temperature which has subsequently solidified as fayalite.

Figure 42 illustrates the typical structure of the reaction interface from the 4.10% manganese alloy cast in a greensand mold. There is extensive fayalite from the liquid silicate melt as well as magnetite and hematite. Figure 43 is the same composition alloy, 4.40% manganese, poured into a shell mold. The sintered layer contains some fayalite from the liquid silicate melt and some spherical metallic crystals in the zone of the prior silicate melt.

The structure in the 0.75% manganese alloys are the same. The greensand sintered layer reveals extensive reaction. The shell sand sintered layer indicates slight reaction with considerable reduction of iron from the silicate melt.

The duplex molds containing shell sand drag and greensand cope substantiate the results of the first series of castings. Figure 44 is the sintered layer from the greensand cope of the 8.60% manganese alloy. The extensive reaction zone contains fayalite and magnetite. The shell mold drag section of the same casting exhibits a sintered layer typified by Figure 45. There is slight reaction as evidenced by fayalite, but there is extensive iron reduction on cooling the liquid silicate melt.

DISCUSSION OF RESULTS

The discussion of the results of this investigation will be divided into the following major sections:

(1) discussion of laboratory equilibration results, and

(2) discussion of engineering significance.

Discussion of Laboratory Equilibration Results

The laboratory equilibration results will be reviewed in the same categories as in the previous section of results.

Iron-Silica Equilibria

The experimental data combined with the available thermodynamic data permit the equilibrium diagram of Darken to be expanded. Since the location of three additional univariant equilibria curves has been determined Figure 1 may be modified to include this information. Figure 46 contains the results of this additional work and includes the location of the following equilibria:

(a) solid metal, liquid metal, silica, gas

(b) solid metal, liquid silicate melt, silica, gas

(c) liquid metal, liquid silicate melt, silica, gas

(d) quintuple point-liquid metal, solid metal, liquid silicate melt, silica, gas.

This modified equilibrium diagram now contains the information that is necessary to determine the effect of temperature and atmosphere on iron-silica interface reaction over the temperature range normally experienced in cast metals practice.

The predicted univariant equilibria solid metal, liquid silicate melt, silica, gas, of Darken is in good agreement with the experimental results of this investigation at lower temperatures. As the quintuple point is approached, i.e., above 1500°C, the experimental curve departs from the calculated approximate curve. This departure is due to the depression of the activity of the iron oxide in the silica saturated slag. Darken assumed a reduction of oxygen activity to one third the equilibrium value due to the presence of the excess silica. In view of the experimental results the actual position of the quintuple point may be more accurately predicted and the oxygen activity approximated.

The position of the univariant equilibrium (a) is indicated by a dashed line since it has been located by calculation. The intersection of curves (a) and (b) then approximates the position of the quintuple point.

Finally, a portion of univariant curve (c) is determined by the quintuple point and the experimental data of this and prior work.

Ferrous Oxide Activity

The activity of the ferrous oxide in the liquid silicate melt may be evaluated in the light of these latest data. The value for log p_{CO_2}/p_{CO} for the quintuple point may be estimated from the revised

equilibrium diagram, Figure 46. With the equilibrium value the activity of the ferrous oxide may be approximated and compared to the value of the activity in the absence of silica. It can be seen that the value of log p_{CO_2}/p_{CO} is greatly depressed by the presence of this excess silica from log p_{CO_2}/p_{CO} = -0.68 to log $p_{CO_2}/p_{CO} \cong$ -1.42. This depression is between 1/5 and 1/6 of the equilibrium ratio in the absence of silica, and differs from Darken's estimated 1/3 value by slightly less than a factor of two. This essentially means that the atmosphere must be even more reducing to prevent the formation of a liquid silicate melt than previously estimated.

The position of the univariant equilibrium liquid metal, liquid silicate melt, silica, gas, is considerably more reducing than previously estimated by an extrapolation of the calculated curve of Darken. From a cast metals point of view this is most significant and unfortunate.

Effect of Manganese Additions

The addition of manganese to the system under investigation increases the degrees of freedom or variance by one for all equilibria. In the case of univariant equilibria (b) and (c) we would have these phases in equilibrium over a range of temperature at a fixed gas composition. Or at a fixed temperature the metallic alloy, solid or liquid, would be in equilibrium with the liquid silicate melt over a range of atmosphere.

The 1% manganese alloy allows the liquid silicate melt to remain stable to extremely reducing atmospheres. At the same time it also low-

ers the stability of the iron-manganese alloy to more reducing conditions.

The 9.85% manganese alloy exhibited the same behavior as the 1% manganese alloy with respect to iron-manganese stability. The atmosphere must be more reducing in the presence of manganese to permit the presence of a stable metallic phase. Under the conditions of this investigation it was impossible to prevent the formation of a liquid silicate melt in the presence of a 9.85% manganese alloy.

The results have great practical significance in the area of cast metal production, and are schematically summarized in Figure 47. The curves are presented on this equilibrium diagram only as a means of comparing the results with the pure iron-carbon alloy and are not necessarily univariant curves. It can be readily seen that additions of manganese to the iron base alloy greatly aggravate the severity and facilitate the occurrence of a mold-metal interface reaction.

Discussion of Engineering Significance

The engineering significance of this investigation will be discussed in the following order:

(a) penetration and interface reaction

(b) problem of manganese additions

(c) effect of mold material

Penetration and Interface Reaction

As noted in the review of the literature there are two possible causes

of metal penetration in a silica mold. Simple mechanical penetration may be a result of pressure exceeding the interfacial energy at the mold wall and causing the liquid metal to fill the interstices of the mold. In addition, however, chemical reaction at the interface may cause the mold wall to break down and allow metal penetration at very low pressures.

There is extensive reference by earlier investigators to the formation of a low melting point slag at the mold-metal interface, but there is considerable confusion between the penetration of metal and the penetration of the low melting point slag. The same confusion has existed with respect to the terms reducing and oxidizing atmosphere and the effect of these atmospheres on reaction and penetration.

The results of this investigation clearly define the role of atmosphere in reaction and penetration. With pure iron-carbon alloys the equilibrium diagram, Figure 46 presents the range of atmosphere control necessary to prevent interface reaction, i.e., the formation of a liquid silicate melt. By converting the CO_2/CO gas ratios to effective p_{O_2} it is obvious that normal cast metal practice operates above the boundaries between liquid silicate melt - solid and liquid iron. The result is that extensive liquid silicate melt formation is experienced with resultant loss of surface smoothness and detail.

The possibility of preventing interface reaction by the introduction of neutral or reducing gases in a mold is, therefore, very slight and most impractical. Even vacuum treatment is not a potential solution. Atmospheres experienced in normal practice should more properly be clas-

sified on a relative oxidizing power basis.

The problem of metal penetration is quite severe in heavy castings, but it can be a serious problem in small castings, also. Prior investigators have indicated that under oxidizing conditions the metal might wet the silica grains and facilitate penetration. The present work proves that the formation of a liquid silicate melt, in itself, does not cause a great decrease in the interfacial energy between the liquid metal and solid silica. This is confirmed by the analogous results of Atterton.[7] The liquid silicate melt does however attack the mold wall and greatly enlarge the pore size of the silica compact. This will allow metal penetration at very low pressures. Figure 18 clearly shows this mechanism in operation. This sample of iron-silica charge was treated at 1550°C (2822°F) under oxidizing conditions, 3.9% CO_2. The sample size precludes pressure as an important variable. The results of the mold wall attack have allowed metal penetration to completely surround some silica grains. The same size sample at 1550°C (2822°F) under reducing conditions, 3.3% CO_2 exhibited no reaction or penetration.

The Problem of Manganese Additions

The information derived from this investigation with respect to manganese content of the metal is very significant. For many years it has been appreciated that manganese additions to molten alloys greatly aggravate the problem of producing castings with satisfactory surface finish. The experimental results of this work explain the reason for this difficulty. The effect of manganese on the stability of a silicate melt is

graphically illustrated by the equilibrium data. Even very small additions, 1% manganese, greatly lower the reducing tendency of a given gas mixture. It is essentially impossible, therefore, under the conditions investigated to prevent the formation of a liquid silicate melt in the presence of manganese. The higher the level of manganese addition to the iron-base alloy the more severe is the interface reaction. This is verified in practice by the extremely severe mold wall attack of the cast Hadfield steels, 13% manganese. In view of these results extensive use of manganese to improve hardenability or wear resistance in cast iron-carbon alloys should be avoided if good surface finish is a prime requirement.

Effect of Mold Material

The effect of mold material and resultant atmosphere is demonstrated by the results of this investigation. Practically speaking, it is impossible to attempt to control the mold atmosphere by introducing inert or reducing gas mixtures into a mold cavity. The comparative results of green sand molds and shell molds, however, hold some promise. In all cases the use of a sand mixture bonded by a polymerized phenolic resin yielded good cast surfaces, little reaction and improved fluidity. This was true at all levels of manganese additions, 0.23% - 8.60%. Increasing manganese content had a less severe effect on the interface reaction in the resin bonded shell molds than in the greensand molds. Actually the severity of the reaction in the greensand mold was more pronounced at 0.19% manganese than the reaction in the shell mold containing the 8.60%

manganese-iron alloy.

The effect of manganese content on interface reaction in a given type of mold is evident from these experimental castings, also. In both greensand and shell molded castings the degree of liquid silicate melt formation increased with increasing manganese content.

Microscopic investigation of the sintered layers from these castings provided valuable information. The sintered layers removed from the oxidizing greensand interface of all the test castings contained extensive fayalite formed from the liquid silicate melt. In addition these reaction zones contained magnetite and some hematite. The extreme oxidizing nature of this atmosphere can be evaluated by referring to Figure 1. In order to produce these higher oxides of iron on cooling the atmosphere must be considerably more oxidizing than the range of mixtures used in the equilibration investigations.

In contrast to this behavior, the reaction zones removed from the shell molded castings contained products identical to the equilibration samples. The presence of fayalite confirmed the existence of a liquid silicate melt, but the extensive amount of iron reduced from the silicate melt on cooling indicates the relative reducing nature of the atmosphere.

Since the same result was produced in a duplex mold with a greensand cope and shell sand drag, control of mold atmosphere at the interface may be possible. Organic sand binders similar to the phenolic resin used in this investigation may be a means of minimizing the undersirable interface reaction.

CONCLUSIONS

The results of the equilibrium investigation have determined the location of the important univariant curves in the system iron-silicon-oxygen-carbon under the conditions of interest in cast metals practice. The resultant microstructures explain the nature of mold-metal interface reaction. Under oxidizing conditions a liquid silicate melt is formed and rapidly dissolves the silica mold wall. At temperatures above the melting point of iron this attack may permit the penetration of metal through the chemically enlarged pores of the silica mold wall. The penetration is not accomplished by a reduction in the metal-silica interfacial energy since no examples of low contact angles, i.e., wetting of the silica by the metal, were produced.

The equilibrium results agree with the available published data at lower temperatures, and allow a more accurate estimation of the activity of iron oxide in a silica saturated slag.

Manganese additions greatly facilitate the formation of a liquid silicate melt. Over the range of temperature and atmosphere experienced in this research it was impossible to prevent a metal-silica interface reaction with molten iron-manganese alloys.

The equilibrium investigation data were evaluated and verified by the pouring of selected step-castings. The effect of an oxidizing mold atmosphere was graphically demonstrated in greensand castings. The sur-

face finish and interface reaction zone exhibited extensive liquid silicate melt formation over the entire range of manganese additions. The more reducing atmosphere produced by phenolic resin-bonded shell molds resulted in very slight interface reaction over the range of manganese content from 0.23% to 8.60%. In all cases the minor severity of the attack and the resultant reaction products indicate that the atmosphere was extremely reducing relative to greensand molds. These results indicate that a practical means of minimizing interface reactions may be possible through organic sand binders which can control the interface atmosphere.

TABLE I

CHEMICAL ANALYSIS OF VACUUM MELTED IRON

Description	Heat Number	Chemical Analysis (weight %)				
		C	O_2	N_2	Ni	Si
Ferrovac Rod 1/2-inch diameter Cold rolled	1P164	0.007	0.0056	0.00013	< 0.001	< 0.005

TABLE II

SUMMARY OF EQUILIBRATION EXPERIMENTS

Sample Number	Material Charged	Temperature, °C	Temperature, °F	Time, hours	Gas Analysis, % CO_2	Gas Analysis, % CO	log $\frac{P_{CO_2}}{P_{CO}}$	Microscopic Observations Stable Condensed Phases at Temperature
A-35	Iron-Silica			2.0	5.5	94.5	-1.466	Iron, Silica
A-36	Iron-Silica			1.0	16.2	83.7	-0.713	Melt, Silica
A-37	Iron-1% Manganese-Silica			1.0	9.8	91.2	-0.968	Iron-Manganese, Silica
A-38	Iron-9.85% Manganese-Silica			2.0	8.4	91.6	-1.037	Iron-Manganese, Melt, Silica
A-39	Iron-Silica			2.0	14.2	85.8	-0.781	Melt-Silica
A-40	Iron-1% Manganese-Silica			1.0	11.45	88.55	-0.888	Melt-Silica
A-41	Iron-Silica			1.0	11.7	88.3	-0.878	Bad Sample
A-42	Iron-Silica			2.0	10.5	89.5	-0.930	Iron-Silica
A-43	Iron-1% Manganese-Silica			2.0	10.5	89.5	-0.930	Iron-Manganese, Melt, Silica
A-44	Iron-Silica			2.0	8.4	91.6	-1.037	Iron-Silica
A-45	Iron-1% Manganese-Silica			2.0	8.4	91.6	-1.037	Iron-Manganese, Silica
A-46	Iron-Silica			2.0	9.2	90.8	-0.995	Iron-Silica
A-47	Iron-1% Manganese-Silica	1250	(2282)	2.0	10.0	90.0	-0.954	Iron-Manganese, Silica
A-48	Iron-Silica			2.0	11.0	89.0	-0.908	Iron-Silica
A-49	Iron-Silica			2.0	12.3	87.7	-0.852	Melt, Silica
A-50	Iron-9.85% Manganese-Silica			2.0	7.1	92.9	-1.116	Iron-Manganese, Melt, Silica
A-51	Iron-9.85% Manganese-Silica			2.0	5.9	94.1	-1.202	Iron-Manganese, Melt, Silica
A-52	Iron-9.85% Manganese-Silica			2.0	4.7	95.3	-1.299	Iron-Manganese, Melt, Silica
A-53	Iron-9.85% Manganese-Silica			2.0	3.9	96.1	-1.391	Iron-Manganese, Melt, Silica
A-54	Iron-9.85% Manganese-Silica			2.0	0.2	99.8	-2.698	Iron-Manganese, Melt, Silica
A-55	Iron-Silica			2.0	11.4	88.6	-0.890	Iron-Silica
A-56	Silicate-Silica (Iron)			3.5	10.6	89.4	-0.926	Iron-Silica
A-57	Silicate-Silica (1% Manganese)			3.5	10.6	89.4	-0.926	Melt, Silica
A-58	Silicate-Silica (1% Manganese)			6.0	9.2	90.8	-0.995	Iron-Manganese, Silica
A-59	Silicate-Silica (Iron)			6.0	9.2	90.8	-0.995	Iron-Silica
A-60	Silicate-Silica (9.85% Manganese)			6.0	9.2	90.8	-0.995	Iron-Manganese, Melt, Silica
B-1	Iron-Silica			2.0	6.3	93.7	-1.182	Iron, Silica
B-2	Iron-Silica			2.0	7.3	92.7	-1.136	Iron, Silica
B-3	Iron-Silica			1.0	7.6	92.4	-1.084	Iron, Silica
B-4	Iron-Silica			2.0	9.9	90.1	-0.959	Melt, Silica
B-5	Silicate-Silica (Iron)			2.5	8.2	91.8	-1.086	Iron, Silica
B-6	Silicate-Silica (Iron)			3.5	5.6	94.4	-1.228	Iron, Silica
B-7	Iron-Silica			3.5	5.6	94.4	-1.228	Iron, Silica
B-8	Iron-9.85% Manganese-Silica			3.25	37	63	-0.232	Melt, Silica
B-9	Iron-1% Manganese-Silica			3.5	37	63	-0.232	Melt, Silica
B-10	Iron-Silica			8.0	37	63	-0.232	Melt, Silica
B-11	Iron-9.85% Manganese-Silica			2.25	0.2	99.8	-2.698	Iron-Manganese, Melt, Silica
B-12	Iron-1% Manganese-Silica	1400	(2552)	3.5	7.3	92.7	-1.103	Iron-Manganese, Melt, Silica
B-13	Silicate-Silica (1% Manganese)			3.5	7.3	92.7	-1.103	Iron-Manganese, Melt, Silica
B-14	Silicate-Silica (9.85% Manganese)			3.5	7.5	92.5	-1.125	Iron-Manganese, Melt, Silica
B-15	Silicate-Silica (1% Manganese)			3.5	7.5	92.5	-1.125	Iron-Manganese, Melt, Silica
B-16	Silicate-Silica (9.85% Manganese)			2.5	9.2	90.8	-0.995	Melt, Silica
B-17	Silicate-Silica (Iron)			2.5	9.2	90.8	-0.995	Iron, Silica
B-18	Iron-1% Manganese-Silica			3.5	5.97	94.03	-1.187	Iron-Manganese, Melt, Silica
B-19	Iron-1% Manganese-Silica			2.0	0.2	99.8	-2.698	Iron-Manganese, Melt, Silica
B-20	Silicate-Silica (9.85% Manganese)			3.5	11.5	88.5	-0.886	Melt, Silica
B-21	Silicate-Silica (Iron)			3.5	11.5	88.5	-0.886	Melt, Silica
B-22	Silicate-Silica (9.85% Manganese)			3.0	10.5	89.5	-0.930	Melt, Silica
B-23	Silicate-Silica (1% Manganese)			3.0	10.5	89.5	-0.930	Melt, Silica
C-1	Iron-1% Manganese-Silica			3.0	37	63	-0.232	Melt, Silica
C-2	Iron-9.85% Manganese-Silica			2.0	37	63	-0.232	Melt, Silica
C-3	Iron-Silica			2.0	37	63	-0.232	Melt, Silica
C-4	Silicate-Silica (Iron)			1.0	6.6	93.4	-1.150	Melt, Silica
C-5	Iron-Silica			1.0	6.6	93.4	-1.150	Melt, Silica
C-6	Iron-Silica			1.0	5.5	94.5	-1.236	Melt, Silica
C-7	Silicate-Silica (Iron)			1.0	5.5	94.5	-1.236	Melt, Silica
C-8	Silicate-Silica (Iron)			1.0	5.0	95.0	-1.278	Iron, Silica
C-9	Iron-Silica			1.0	5.0	95.0	-1.278	Iron, Silica
C-10	Silicate-Silica (1% Manganese)			1.0	4.9	95.1	-1.287	Iron-Manganese, Melt, Silica
C-11	Silicate-Silica (9.85% Manganese)			1.0	4.9	95.1	-1.287	Iron-Manganese, Melt, Silica
C-12	Silicate-Silica (1% Manganese)			2.0	6.7	93.3	-1.143	Melt, Silica
C-13	Silicate-Silica (9.85% Manganese)			2.0	6.7	93.3	-1.143	Melt, Silica
C-14	Silicate-Silica (Iron)	1500	(2732)	2.0	6.7	93.3	-1.143	Melt, Silica
C-15	Iron-1% Manganese-Silica			2.0	0.2	99.8	-2.698	Iron-Manganese, Melt, Silica
C-16	Iron-9.85% Manganese-Silica			2.0	0.2	99.8	-2.698	Iron-Manganese, Melt, Silica
C-17	Silicate-Silica (1% Manganese)			1.0	7.0	93.0	-1.122	Melt, Silica
C-18	Silicate-Silica (9.85% Manganese)			1.0	7.0	93.0	-1.122	Melt, Silica
C-19	Silicate-Silica (1% Manganese)			4.0	6.75	93.25	-1.141	Melt, Silica
C-20	Silicate Silica (9.85% Manganese)			4.0	6.75	93.25	-1.141	Melt, Silica
C-21	Silicate-Silica (9.85% Manganese)			3.0	7.1	92.9	-1.116	Melt, Silica
C-22	Silicate-Silica (9.85% Manganese)			3.0	7.1	92.9	-1.116	Melt, Silica
C-23	Silicate-Silica (1% Manganese)			3.0	8.2	91.8	-1.086	Melt, Silica
C-24	Silicate-Silica (9.85% Manganese)			3.0	8.2	91.8	-1.086	Melt, Silica
C-25	Silicate-Silica (Iron)			3.0	8.2	91.8	-1.086	Melt, Silica
C-26	Silicate-Silica (Iron)			3.0	6.9	93.1	-1.130	Melt, Silica
C-27	Iron-Silica			3.0	6.9	93.1	-1.130	Melt, Silica
D-1	Iron-1% Manganese-Silica			1.0	37	63	-0.232	Melt, Silica
D-2	Iron-9.85% Manganese-Silica			1.0	37	63	-0.232	Melt, Silica
D-3	Iron-Silica			1.0	37	63	-0.232	Melt, Silica
D-4	Silicate-Silica (Iron)			1.0	4.98	95.02	-1.280	Melt, Silica
D-5	Iron-Silica			1.0	4.98	95.02	-1.280	Melt, Silica
D-6	Silicate-Silica (Iron)			1.0	3.9	96.1	-1.391	Melt, Silica
D-7	Iron-Silica	1550	(2822)	1.0	3.9	96.1	-1.391	Melt, Silica
D-8	Silicate-Silica (1% Manganese)			1.5	3.05	96.95	-1.501	Iron-Manganese, Melt, Silica
D-9	Silicate-Silica (9.85% Manganese)			1.5	3.05	96.95	-1.501	Iron-Manganese, Melt, Silica
D-10	Silicate-Silica (Iron)			1.0	3.3	96.7	-1.466	Iron-Silica
D-11	Iron-Silica			1.0	3.3	96.7	-1.466	Iron-Silica
D-12	Iron-1% Manganese-Silica			1.0	0.2	99.8	-2.698	Iron-Manganese, Melt, Silica
D-13	Iron-9.85% Manganese-Silica			1.0	0.2	99.8	-2.698	Iron-Manganese, Melt, Silica

TABLE III

SAND MIXTURES FOR TEST CASTINGS

Description	Constituent	Weight %
Greensand	N.J. Silica Sand 140 mesh	92
	Western Bentonite	3.5
	Mogul Cereal	1
	Water	3.5
Shell Sand	N.J. Silica Sand 140 mesh	95
	Phenolic Resin	5

TABLE IV

SUMMARY OF TEST CASTINGS

Casting Number	Type of Mold	Pouring Temperature, °F	Surface Condition	Chemical Analysis (weight %)				
				C	Mn	Si	P	S
E-1	Greensand	2810	poor surface, extensive reaction	0.16	0.19	0.13	0.011	0.020
E-2	Shell Mold	2760	smooth surface slight reaction	0.20	0.23	0.21	0.014	0.036
E-3	Greensand	2810	poor surface, extensive reaction, low fluidity	0.18	4.10	0.33	0.011	0.019
E-4	Shell Mold	2730	smooth surface, slight reaction, good fluidity	0.20	4.40	0.45	0.010	0.018
E-5	Greensand	2950	extensive reaction, penetration, fusion	0.10	0.75	0.13	0.011	0.021
E-6	Shell Mold	2940	slight reaction, fusion, no penetration	0.12	1.03	0.26	0.013	0.021
E-7	Shell Mold Drag Greensand Cope	2950	slight reaction on drag, extensive reaction on cope	0.16	0.50	0.34	0.012	0.021
E-8	Shell Mold Drag Greensand Cope	2800	slight reaction on drag, extensive reaction on cope	0.15	8.60	0.41	0.010	0.019

TABLE V

CALCULATED UNIVARIANT EQUILIBRIUM

SOLID METAL, LIQUID METAL, SILICA, GAS

% CO_2	$\log \frac{P_{CO_2}}{P_{CO}}$	% C	Temperature, °C
1.0	-1.99	0.241	1525
2.0	-1.69	0.118	1535
2.75	-1.55	0.085	1536

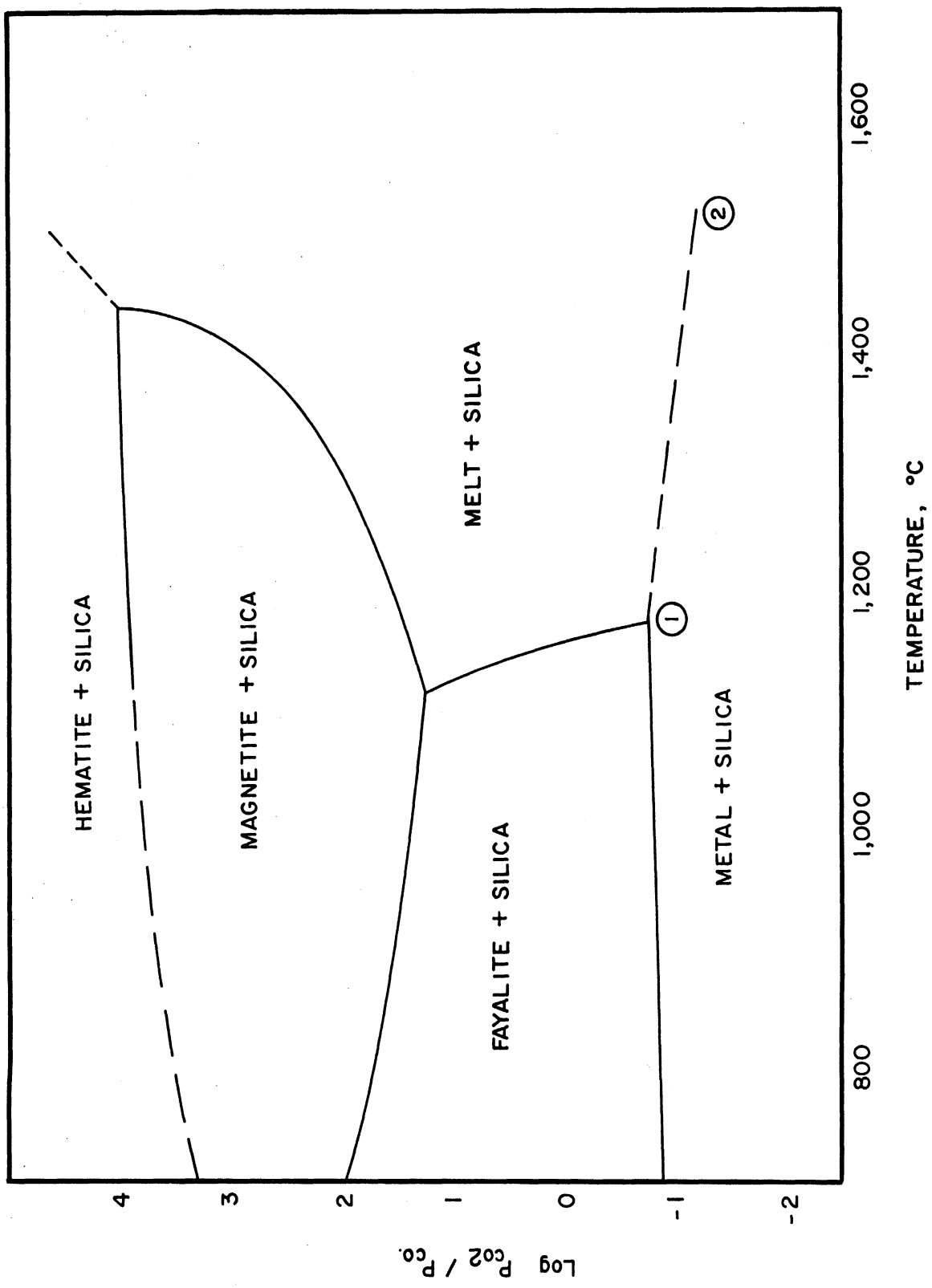

Iron, silicon, oxygen, carbon system
Silica side of the eutectic

Figure 1. Equilibrium diagram after Darken.[16]

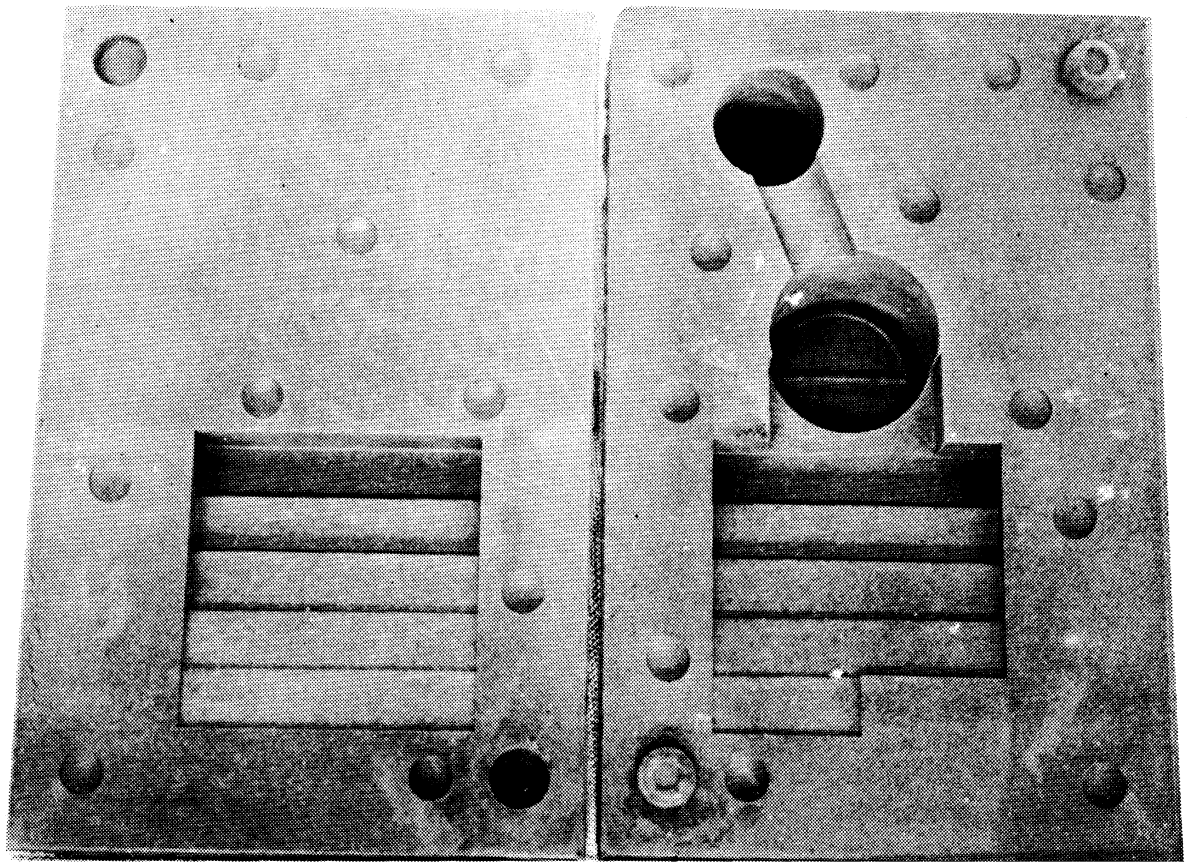

Figure 2. Shell mold for test step-casting.

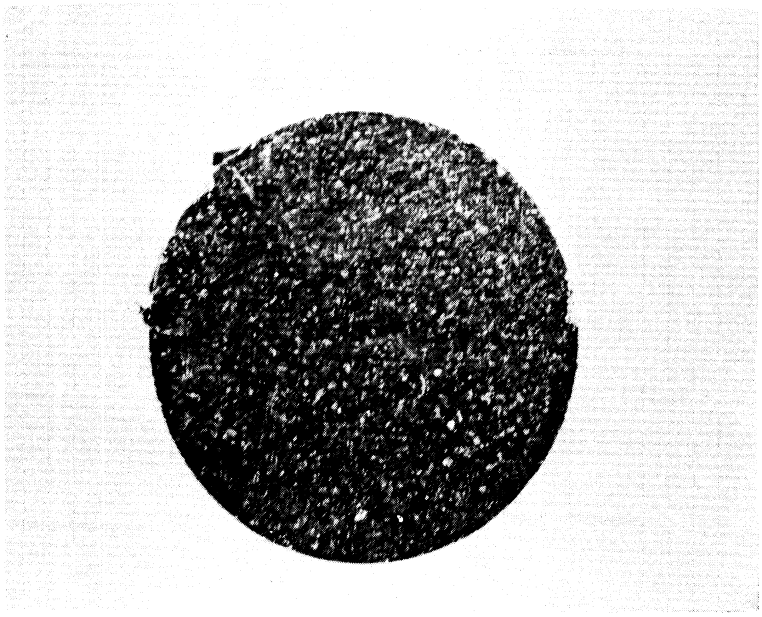

Iron-silica charge
Magnification: 4.5X

1250°C (2282°F) - 2 hr
11.4% CO_2 - 88.6% CO

Figure 3. Surface condition of sample A-55.

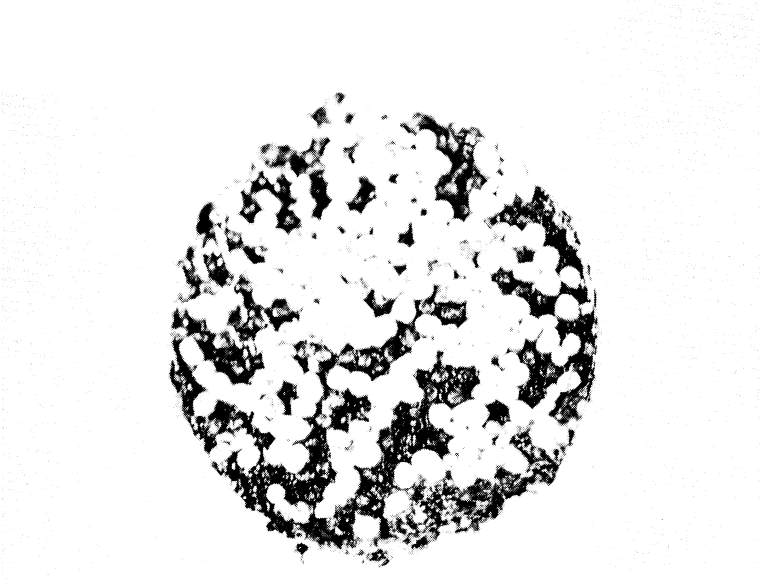

Iron-silica charge
Magnification: 4.5X

1250°C (2282°F) - 2 hr
12.3% CO_2 - 87.7% CO

Figure 4. Surface condition of sample A-49.

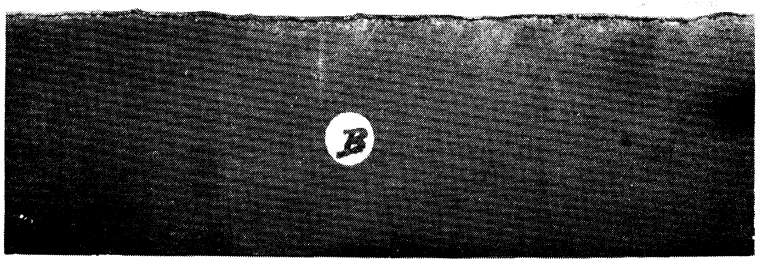

Iron-silica charge — 1250°C (2282°F) - 2 hr
Magnification: 500X — 11.4% CO_2 - 88.6% CO

Figure 5. Microstructure of sample A-55.*

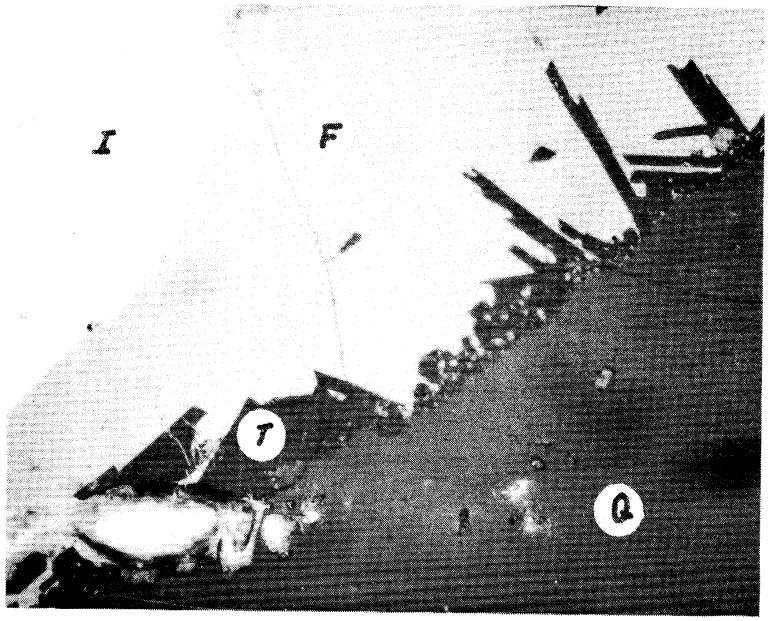

Iron-silica charge — 1250°C (2282°F) - 2 hr
Magnification: 500X — 12.3% CO_2 - 87.7% CO

Figure 6. Microstructure of sample A-49.*

*See Appendix I for code on photomicrographs, page 73.

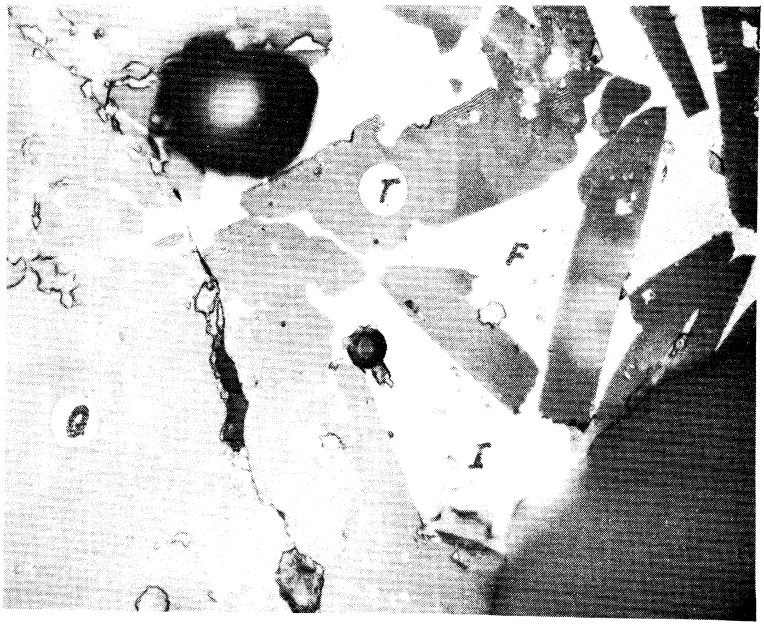

Silicate-silica charge
Magnification: 500X

1400°C (2552°F) - 2.5 hr
9.2% CO_2 - 90.8% CO

Figure 7. Microstructure of sample B-17.

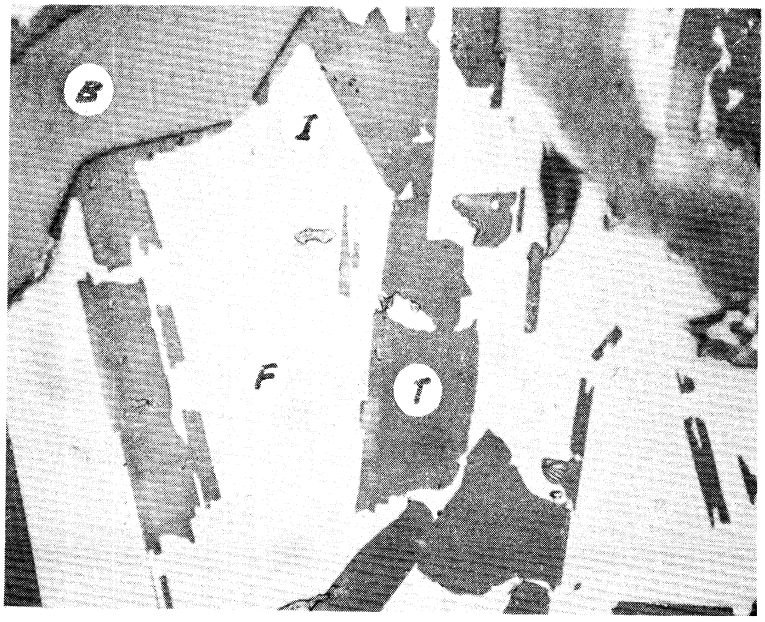

Silicate-silica charge
Magnification: 500X

1400°C (2552°F) - 3.5 hr
11.5% CO_2 - 88.5% CO

Figure 8. Microstructure of sample B-21.

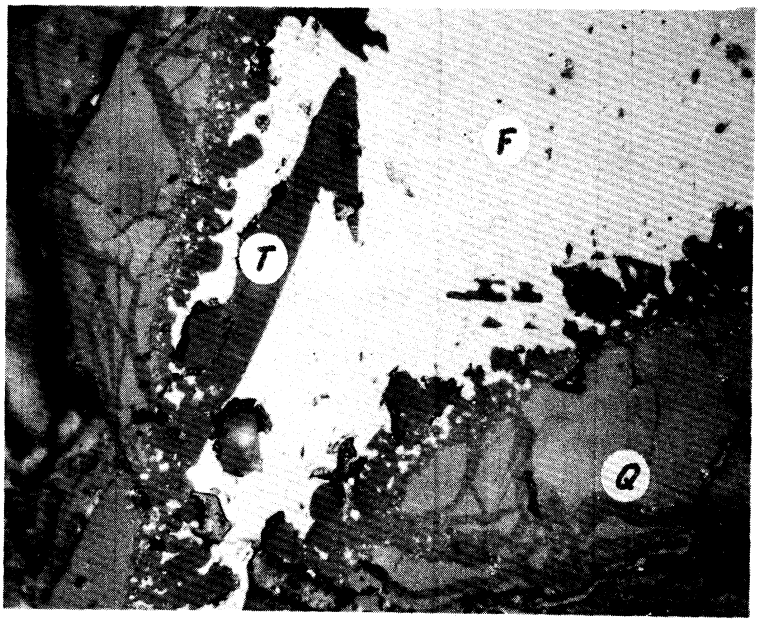

Iron-silica charge
Magnification: 500X

1400°C (2552°F) - 2 hr
9.9% CO_2 - 90.1% CO

Figure 9. Microstructure of sample B-4.

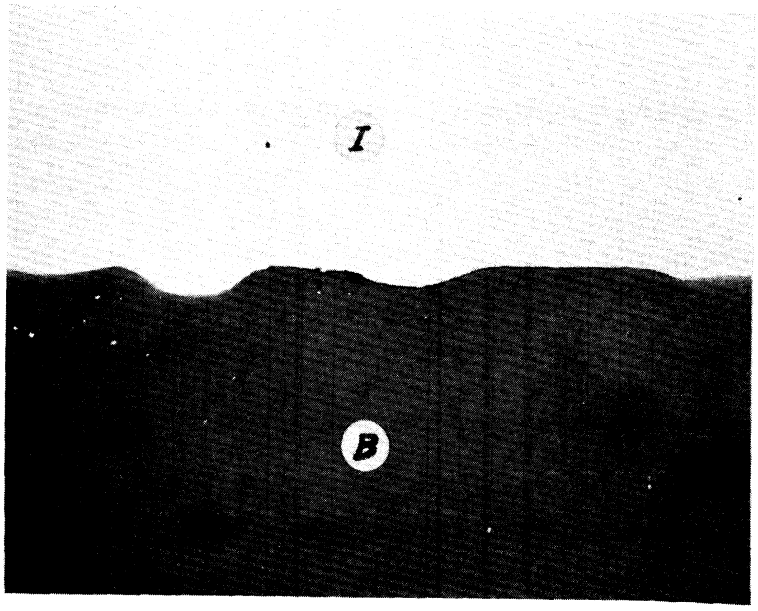

Iron-silica charge
Magnification: 500X

1400°C (2552°F) - 2 hr
7.6% CO_2 - 92.4% CO

Figure 10. Microstructure of sample B-3.

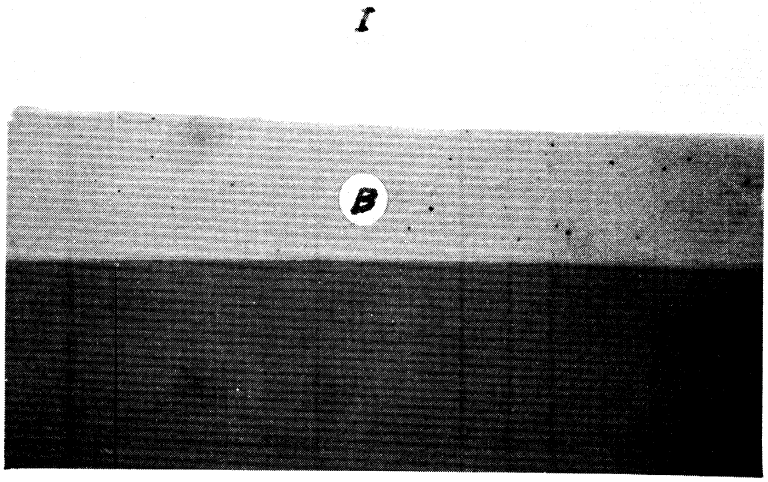

Iron-silica charge
Magnification: 500X

1500°C (2732°F) - 1 hr
5.0% CO_2 - 95.0% CO

Figure 11. Microstructure of sample C-9.

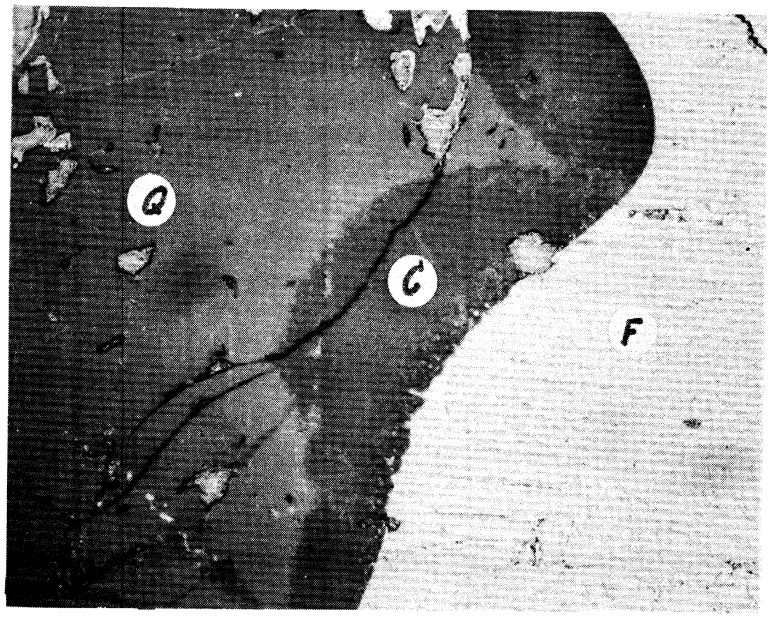

Iron-silica charge
Magnification: 500X

1500°C (2732°F) - 1 hr
5.5% CO_2 - 94.5% CO

Figure 12. Microstructure of sample C-6.

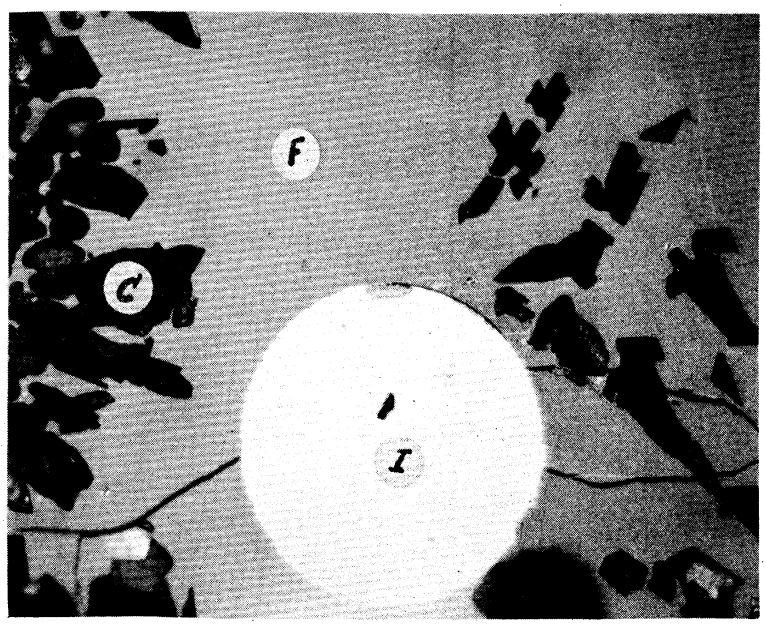

Silicate-silica charge — 1500°C (2732°F) - 1 hr
Magnification: 500X — 5.0% CO_2 - 95.0% CO

Figure 13. Microstructure of sample C-8.

Silicate-silica charge — 1500°C (2732°F) - 1 hr
Magnification: 500X — 5.5% CO_2 - 94.5% CO

Figure 14. Microstructure of sample C-7.

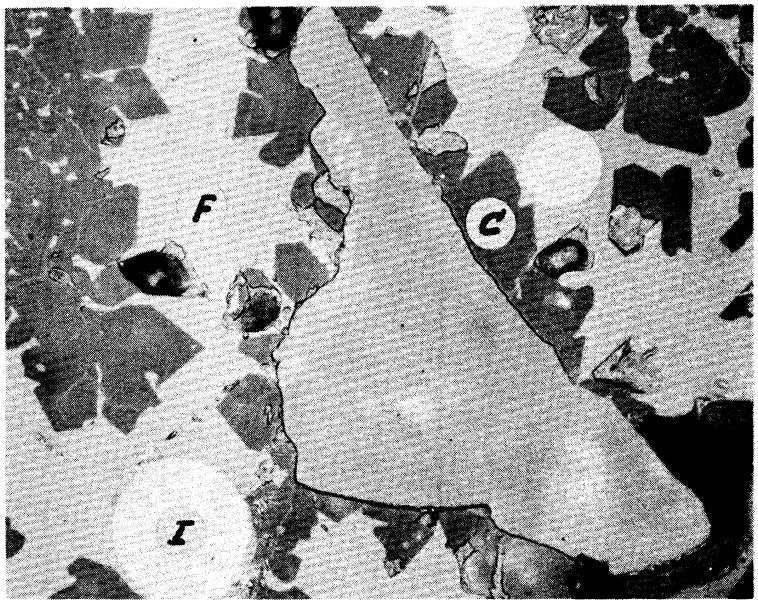

Silicate-silica charge — 1550°C (2822°F) - 1 hr
Magnification: 500X — 3.3% CO_2 - 96.7% CO

Figure 15. Microstructure of sample D-10.

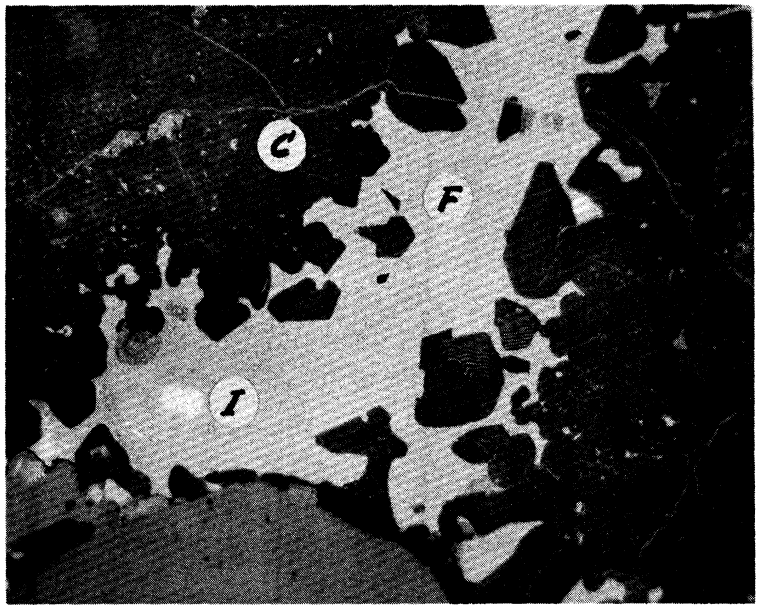

Silicate-silica charge — 1550°C (2882°F) - 1 hr
Magnification: 500X — 4.98% CO_2 - 95.02% CO

Figure 16. Microstructure of sample D-4.

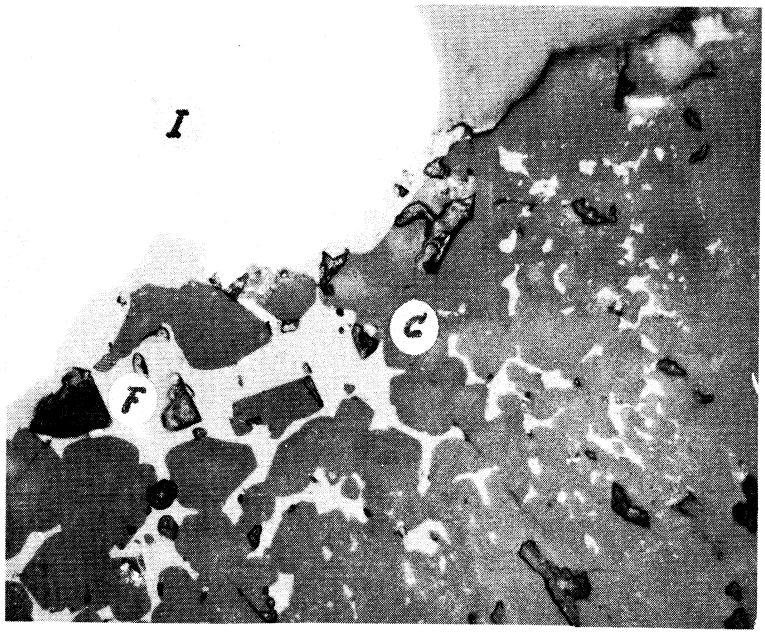

Iron-silica charge
Magnification: 500X

1550°C (2822°F) - 1 hr
3.9% CO_2 - 96.1% CO

Figure 17. Microstructure of sample D-7.

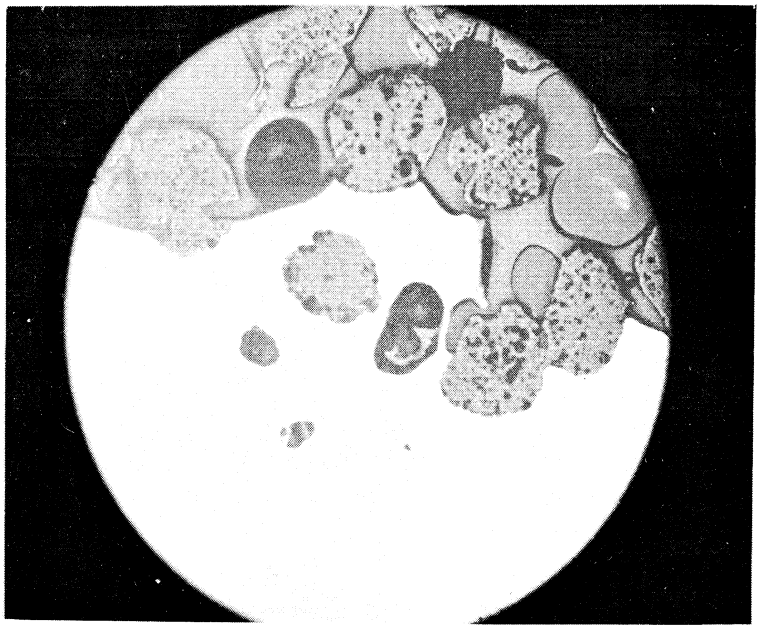

Iron-silica charge
Magnification: 25X

1550°C (2822°F) - 1 hr
3.9% CO_2 - 96.1% CO

Figure 18. Penetration of iron in sample D-7.

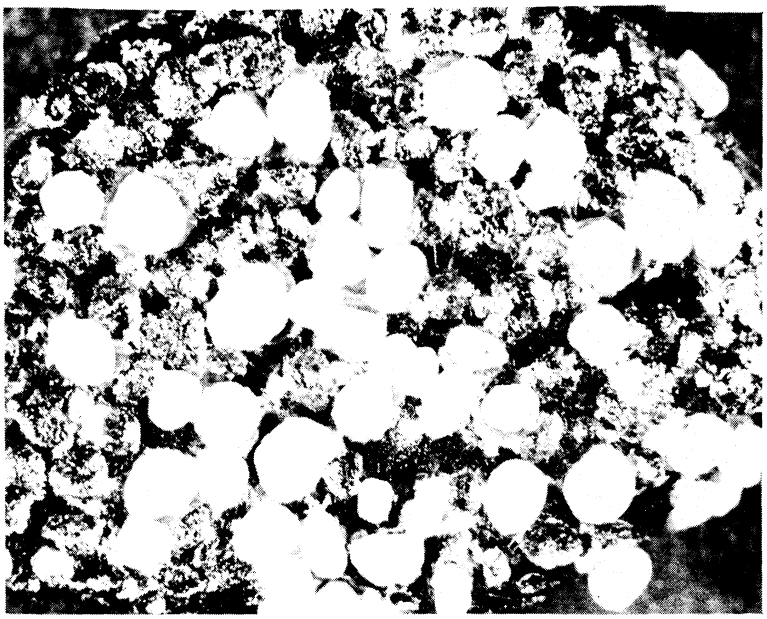

Iron-silica charge
Magnification: 12X

1550°C (2822°F) - 1 hr
3.3% CO_2 - 96.7% CO

Figure 19. Surface condition of sample D-11.

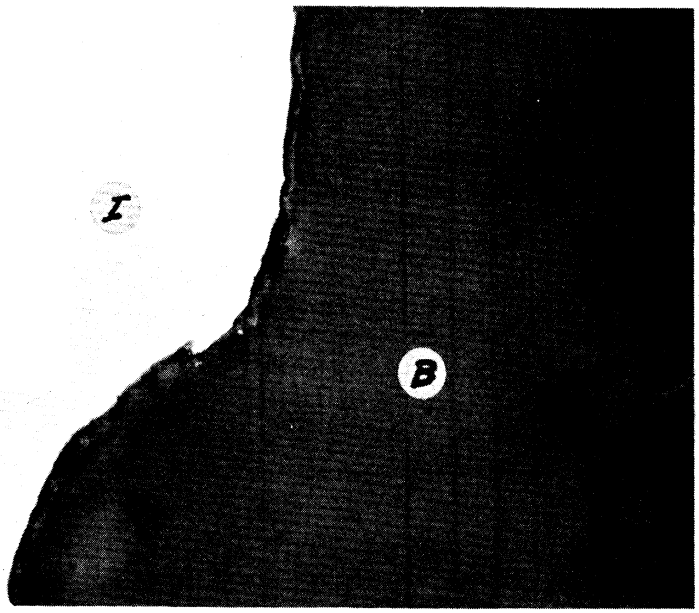

Iron-silica charge
Magnification: 500X

1550°C (2822°F) - 1 hr
3.3% CO_2 - 96.7% CO

Figure 20. Microstructure of sample D-11.

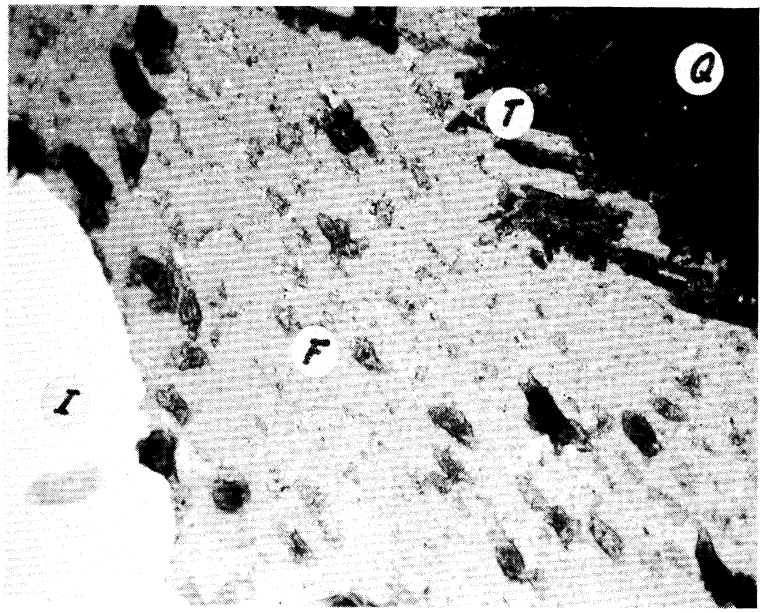

Iron-1% manganese-silica charge — 1250°C (2282°F) - 2 hr
Magnification: 500X — 10.5% CO_2 - 89.5% CO

Figure 21. Microstructure of sample A-43.

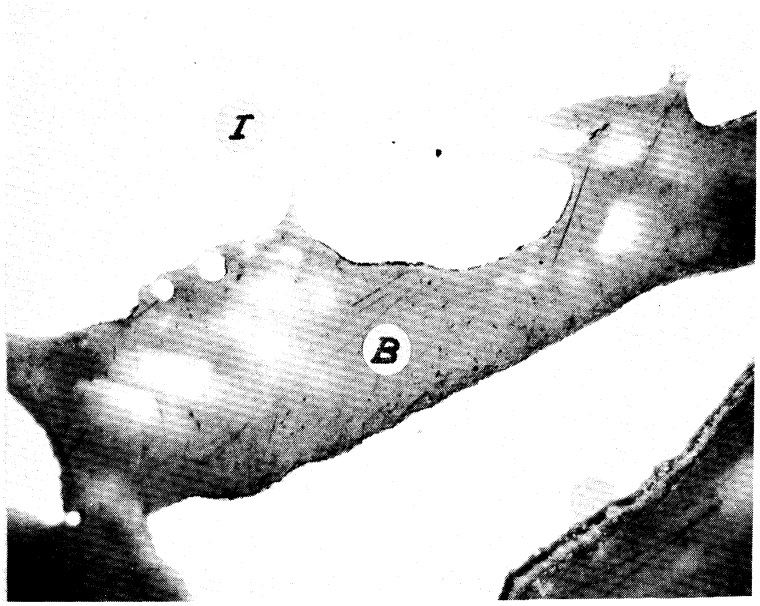

Iron-1% manganese-silica charge — 1250°C (2282°F) - 2 hr
Magnification: 500X — 10.0% CO_2 - 90.0% CO

Figure 22. Microstructure of sample A-47.

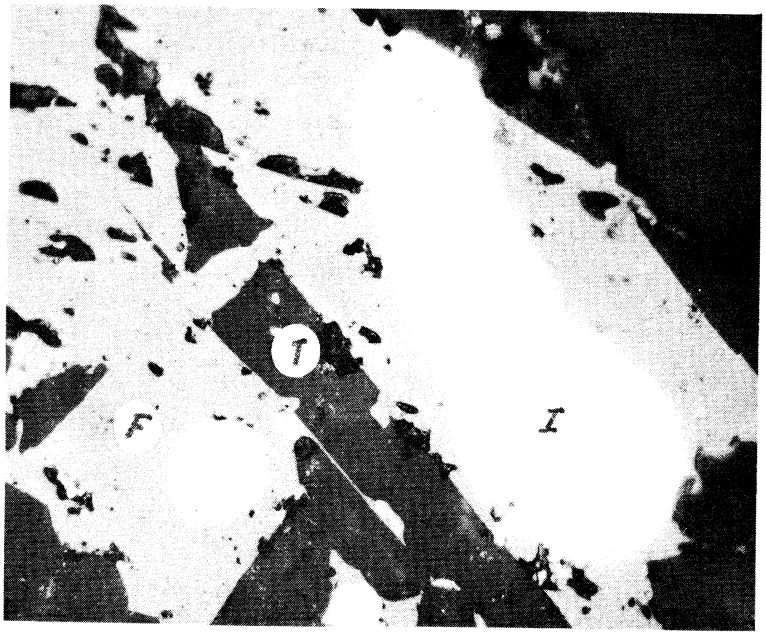

Silicate-silica charge (1% manganese) 1250°C (2282°F) - 6 hr
Magnification: 500X 9.2% CO_2 - 90.8% CO

Figure 23. Microstructure of sample A-58.

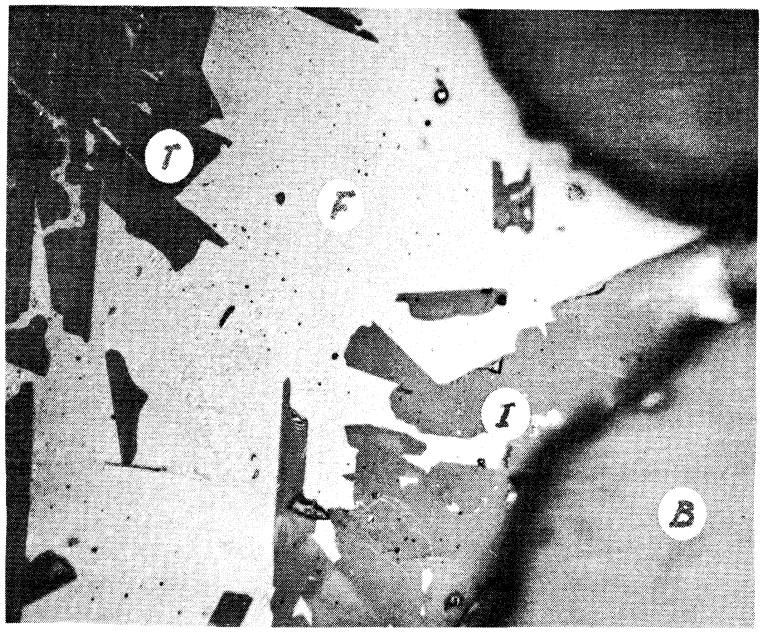

Silicate-silica charge (1% manganese) 1250°C (2282°F) - 3.5 hr
Magnification: 500X 10.6% CO_2 - 89.4% CO

Figure 24. Microstructure of sample A-57.

Iron-1% manganese-silica charge
Magnification: 500X

1400°C (2552 F) - 2 hr
0.2% CO_2 - 99.8% CO

Figure 25. Microstructure of sample B-19.

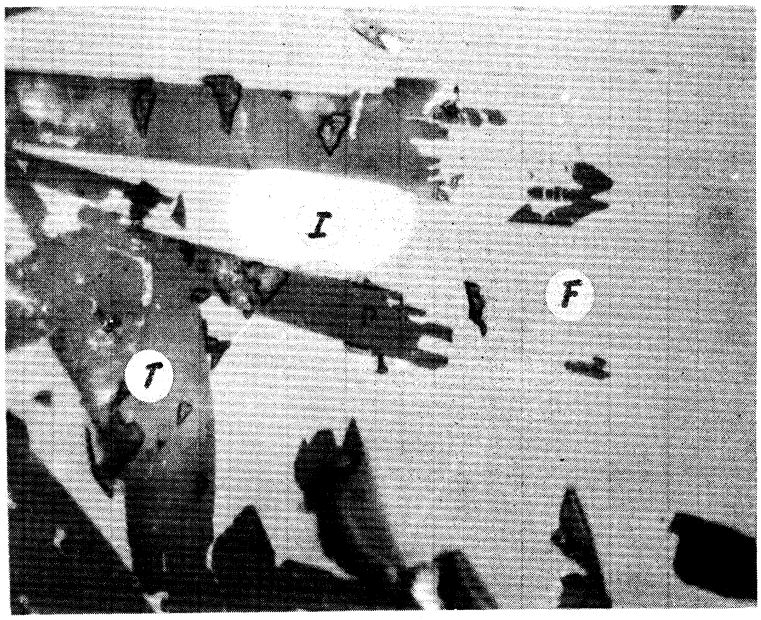

Silicate-silica charge (1% manganese)
Magnification: 500X

1400°C (2552°F) - 3.5 hr
7.5% CO_2 - 92.5% CO

Figure 26. Microstructure of sample B-15.

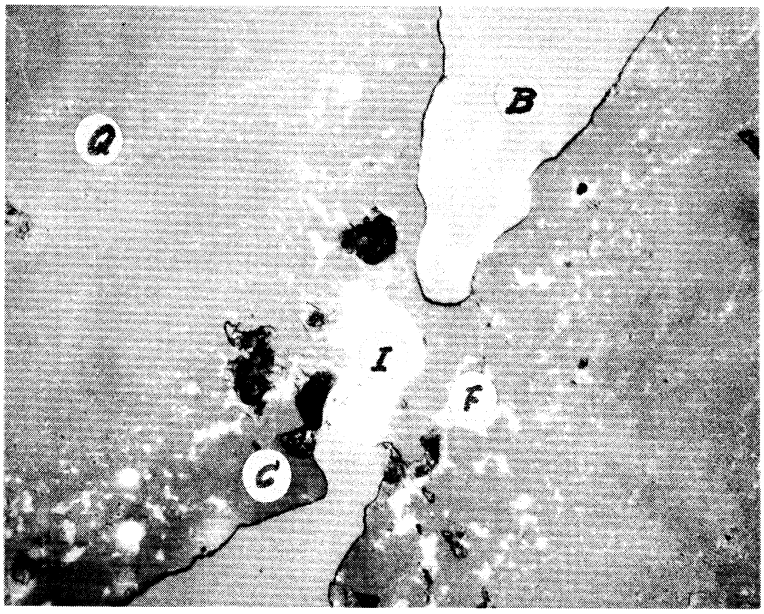

Iron-1% manganese-silica charge — 1500°C (2732°F) - 2 hr
Magnification: 500X — 0.2% CO_2 - 99.8% CO

Figure 27. Microstructure of sample C-15.

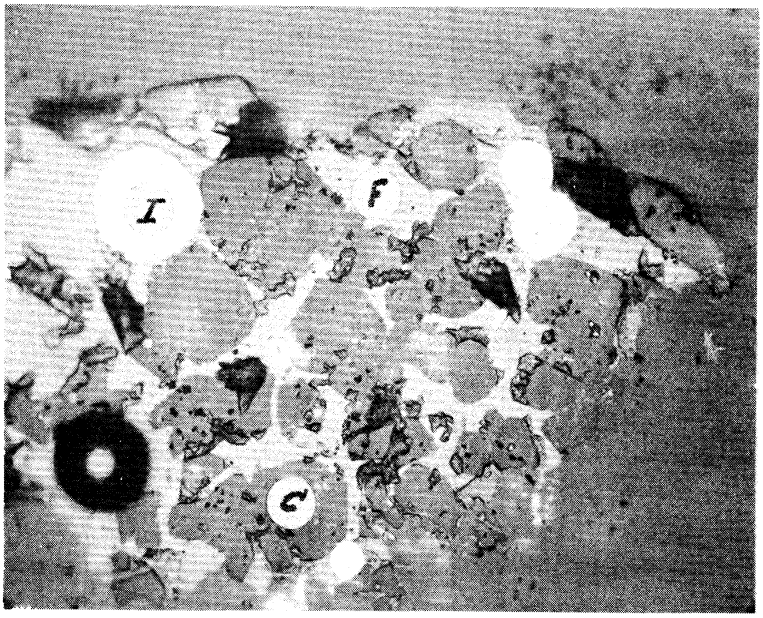

Silicate-silica charge (1% manganese) — 1500°C (2732°F) - 1 hr
Magnification: 500X — 4.9% CO_2 - 95.1% CO

Figure 28. Microstructure of sample C-10.

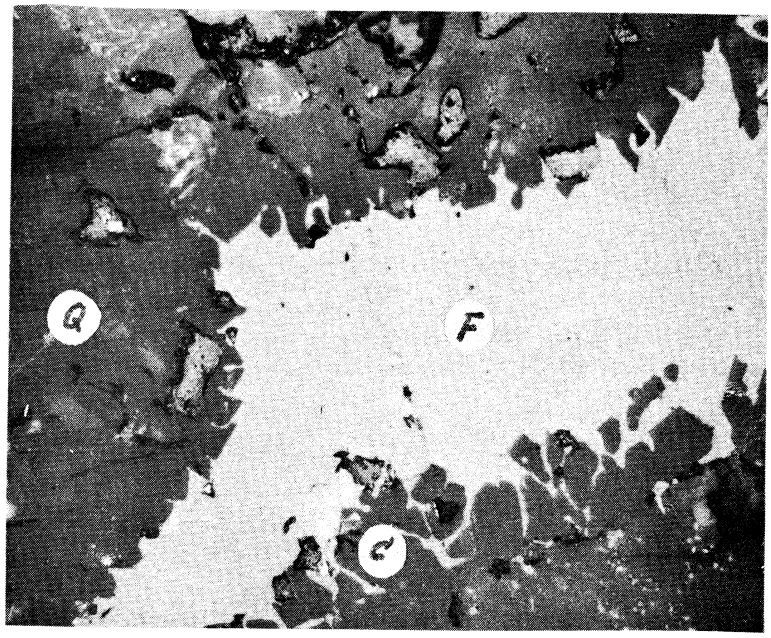

Iron-1% manganese-silica charge
Magnification: 500X

1550°C (2822°F) - 1 hr
0.2% CO_2 - 99.8% CO

Figure 29. Microstructure of sample D-12.

Iron-9.85% manganese-silica charge
Magnification: 500X

1250°C (2282°F) - 2 hr
0.2% CO_2 - 99.8% CO

Figure 30. Microstructure of sample A-54.

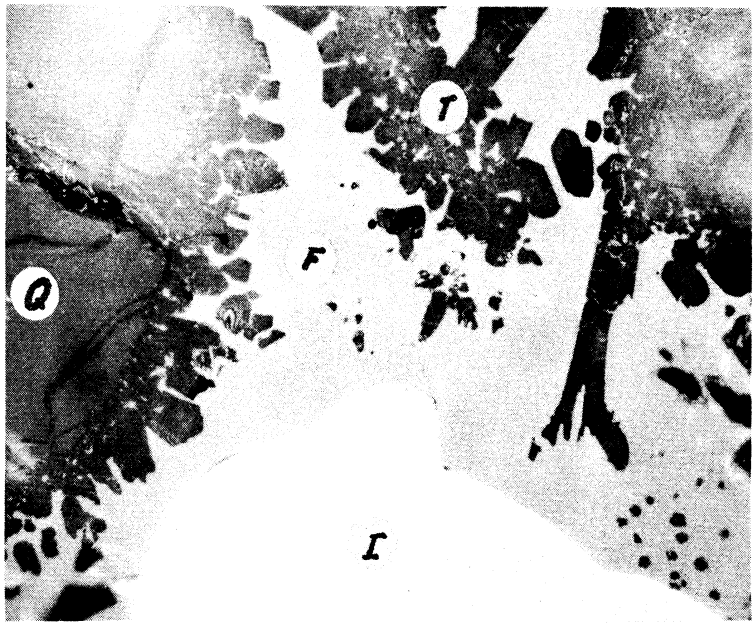

Iron-9.85% manganese-silica charge — 1400°C (2552°F) - 2 hr
Magnification: 500X — 0.2% CO_2 - 99.8% CO

Figure 31. Microstructure of sample B-11.

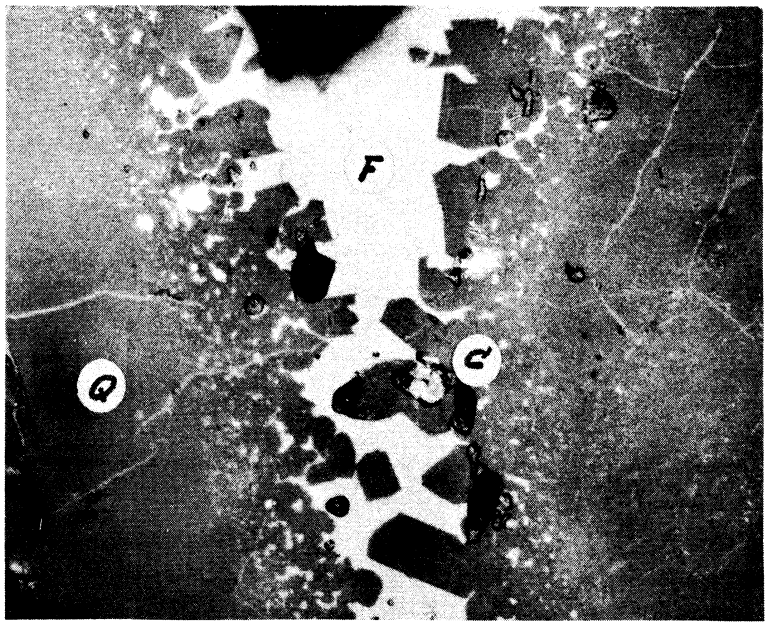

Iron-9.85% manganese-silica charge — 1500°C (2732°F) - 2 hr
Magnification: 500X — 0.2% CO_2 - 99.8% CO

Figure 32. Microstructure of sample C-16.

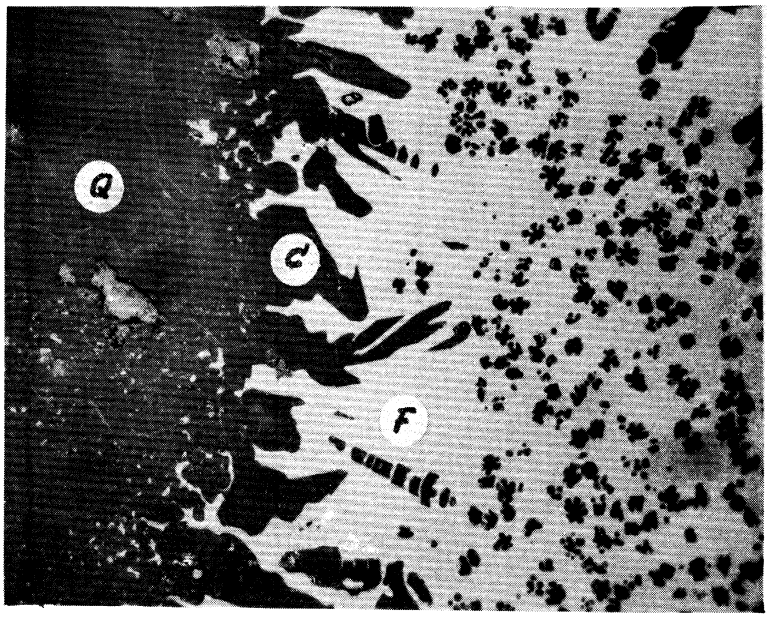

Iron-9.85% manganese-silica charge
Magnification: 500X

1550°C (2822°F) - 1 hr
0.2% CO_2 - 99.8% CO

Figure 33. Microstructure of sample D-13.

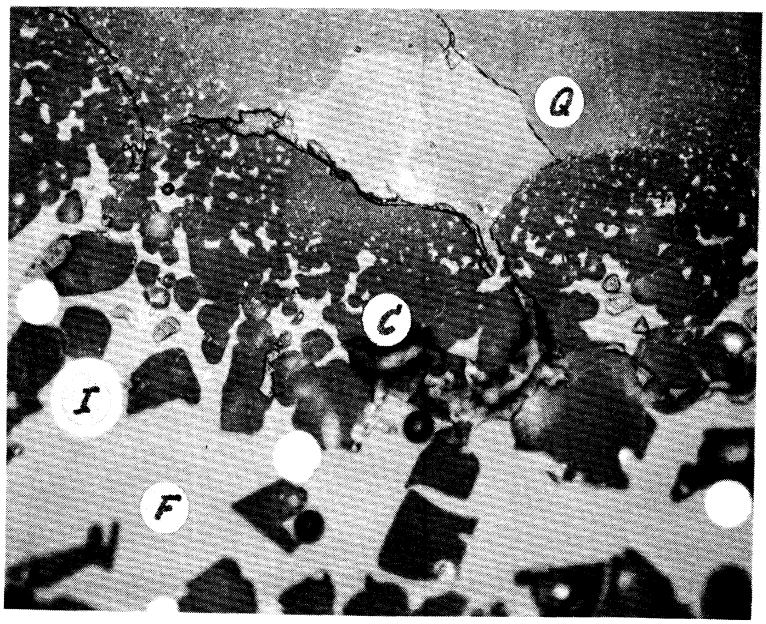

Silicate-silica charge (9.85% manganese)
Magnification: 500X

1500°C (2732°F) - 1 hr
4.9% CO_2 - 95.1% CO

Figure 34. Microstructure of sample C-11.

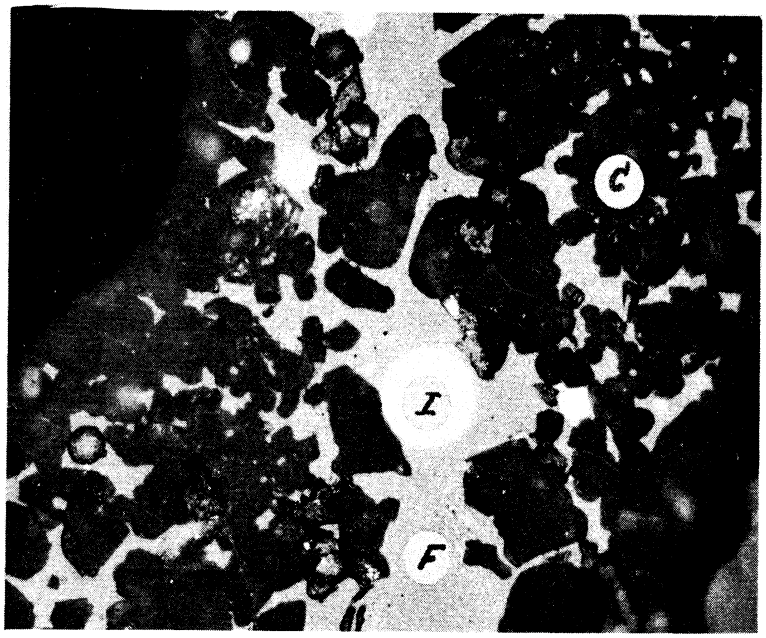

Silicate-silica charge (9.85% manganese) 1550°C (2822°F) - 1.5 hr
Magnification: 500X 3.05% CO_2 - 96.95% CO

Figure 35. Microstructure of sample D-9.

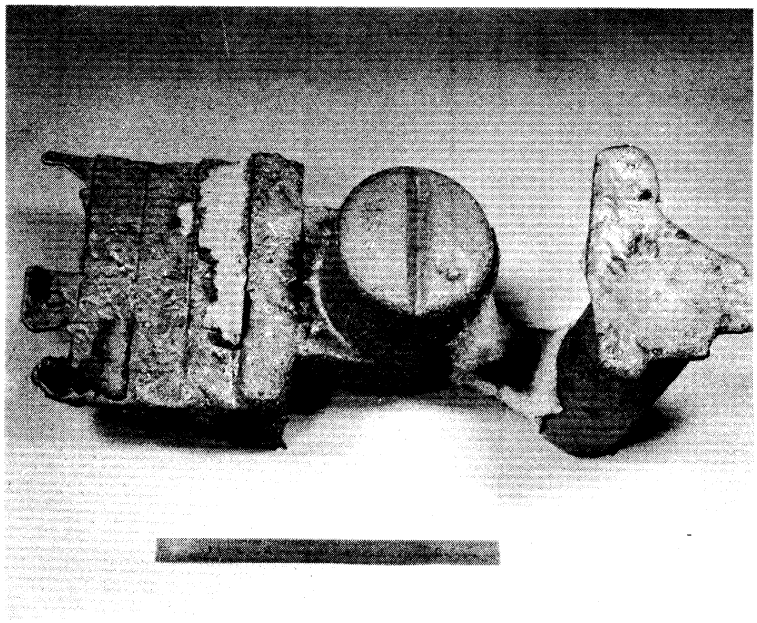

Iron-0.19% manganese alloy Greensand mold

Figure 36. Photograph of test step-casting, E-1.

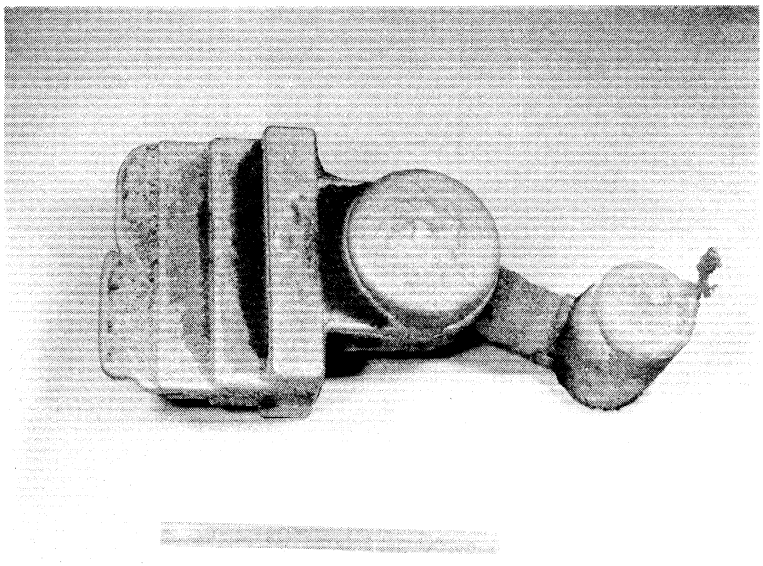

Iron-0.23% manganese alloy Shell sand mold

Figure 37. Photograph of test step-casting, E-2.

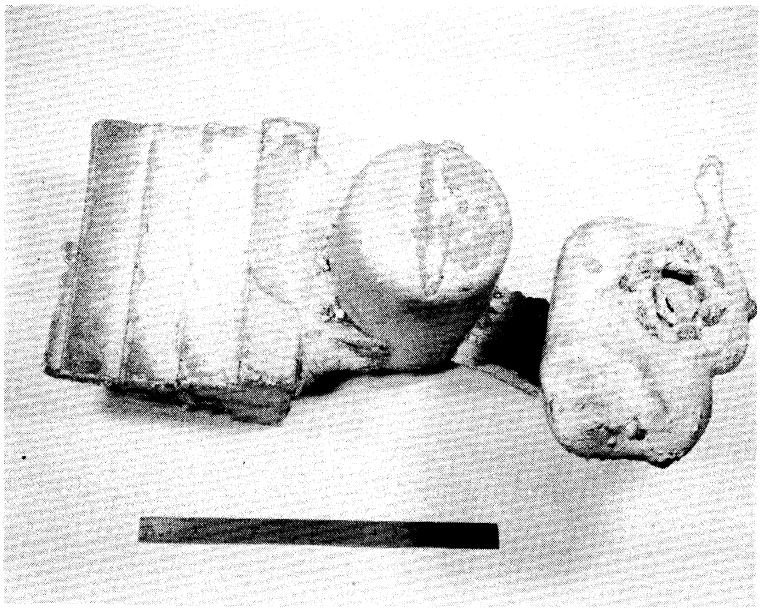

Iron-4.10% manganese alloy Greensand mold

Figure 38. Photograph of test step-casting, E-3.

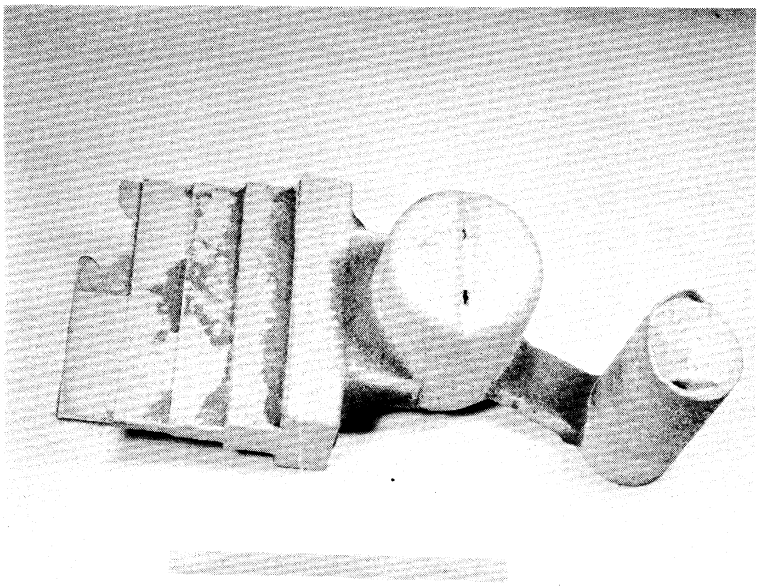

Iron-4.40% manganese alloy Shell sand mold

Figure 39. Photograph of test step-casting, E-4.

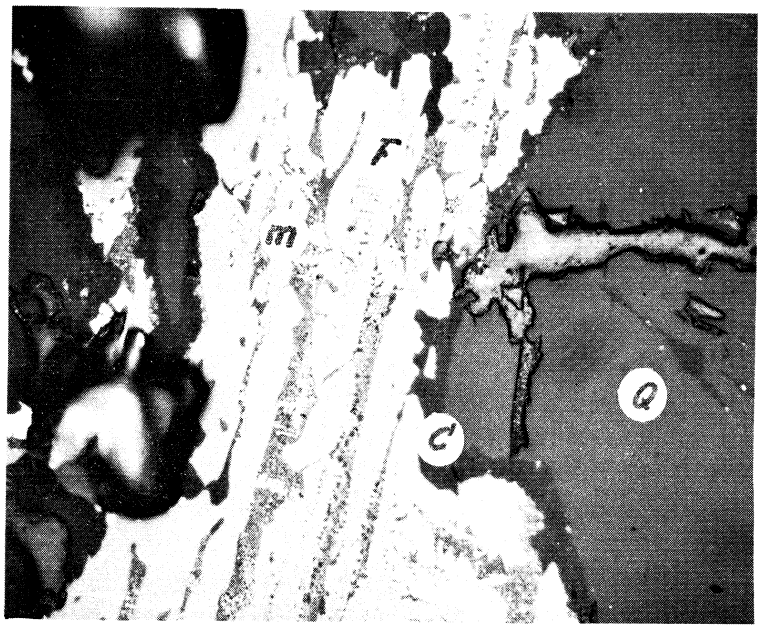

Iron-0.19% manganese alloy — Greensand mold
Magnification: 500X

Figure 40. Microstructure of sintered layer from test step-casting, E-1.

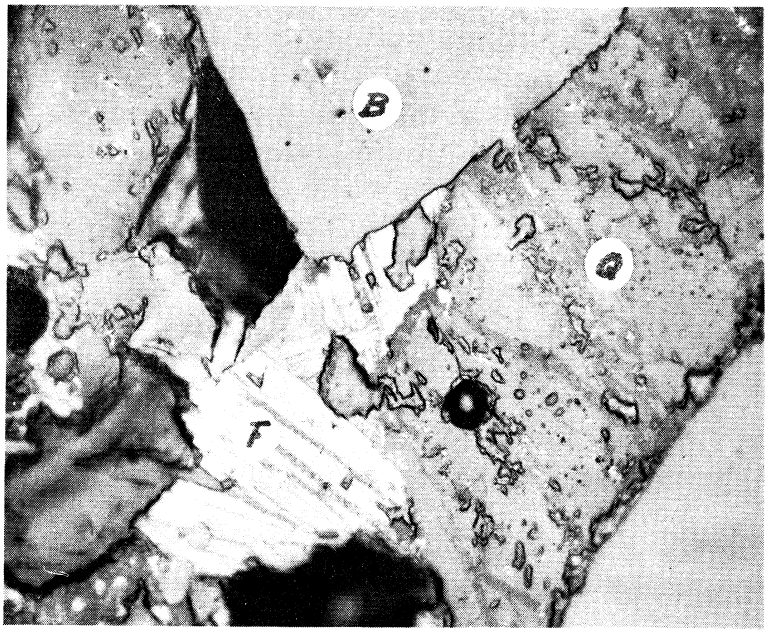

Iron-0.23% manganese alloy — Shell sand mold
Magnification: 500X

Figure 41. Microstructure of sintered layer from test step-casting, E-2.

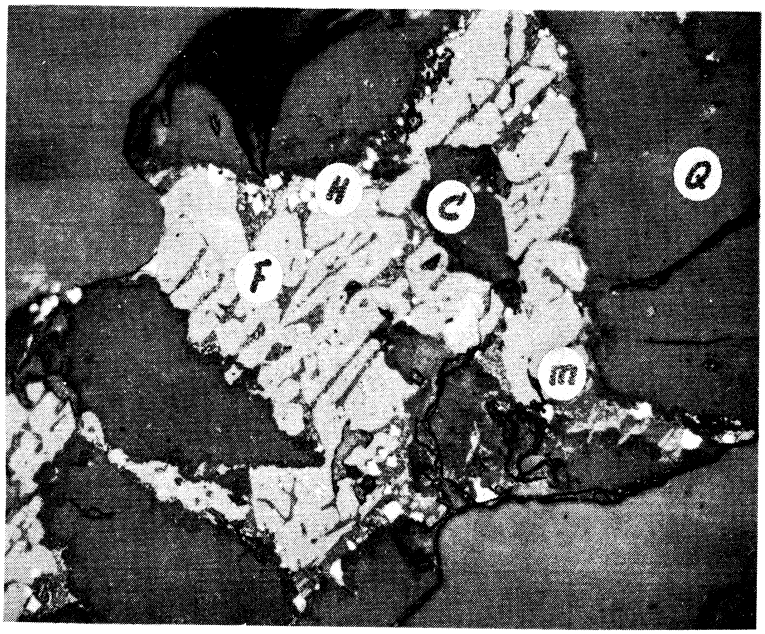

Iron-4.10% manganese alloy Greensand mold
Magnification: 500X

Figure 42. Microstructure of sintered layer from test step-casting, E-3.

Iron-4.40% m .l sand mold
Magnification: 500X

Figure 43. Microstructure of sintered layer from test step-casting, E-4.

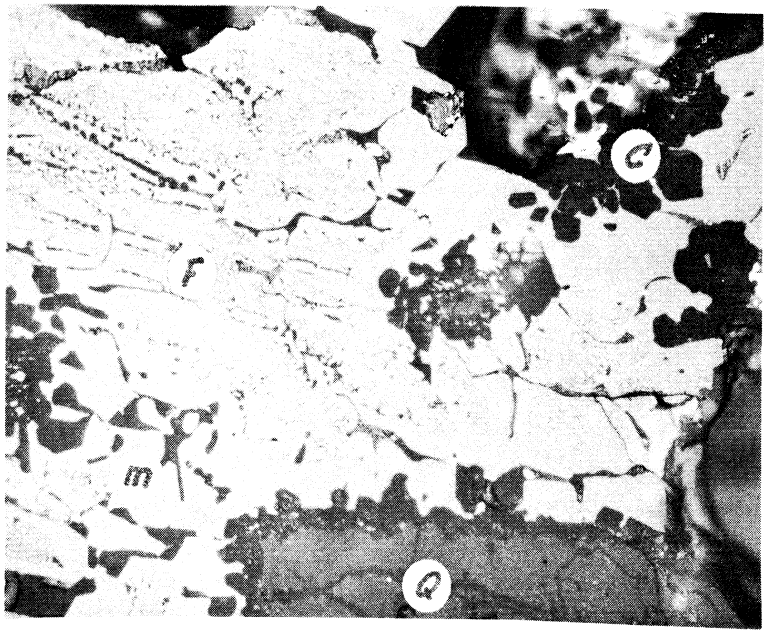

Iron-8.60% manganese alloy — Duplex mold
Magnification: 500X

Figure 44. Microstructure of sintered layer from greensand cope of test step-casting, E-8.

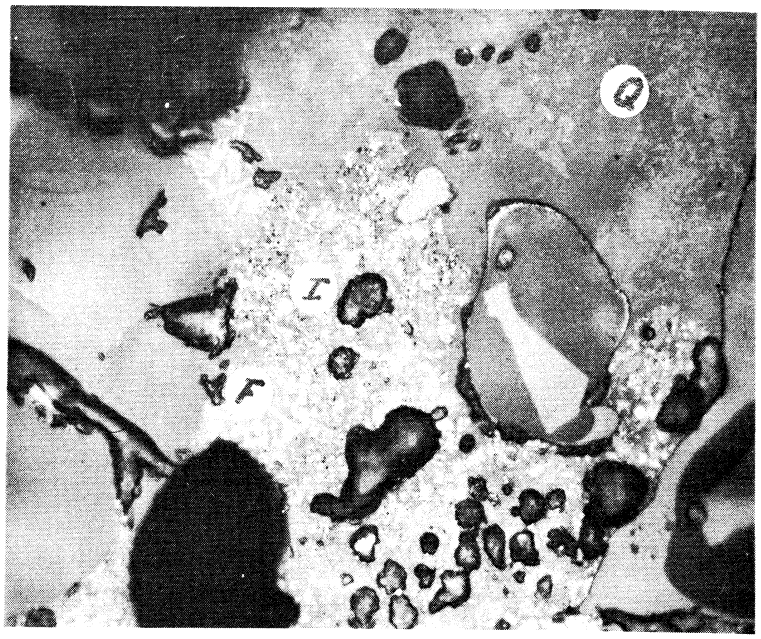

Iron-8.60% manganese alloy — Duplex mold
Magnification: 500X

Figure 45. Microstructure of sintered layer from shell sand drag of test step-casting, E-8.

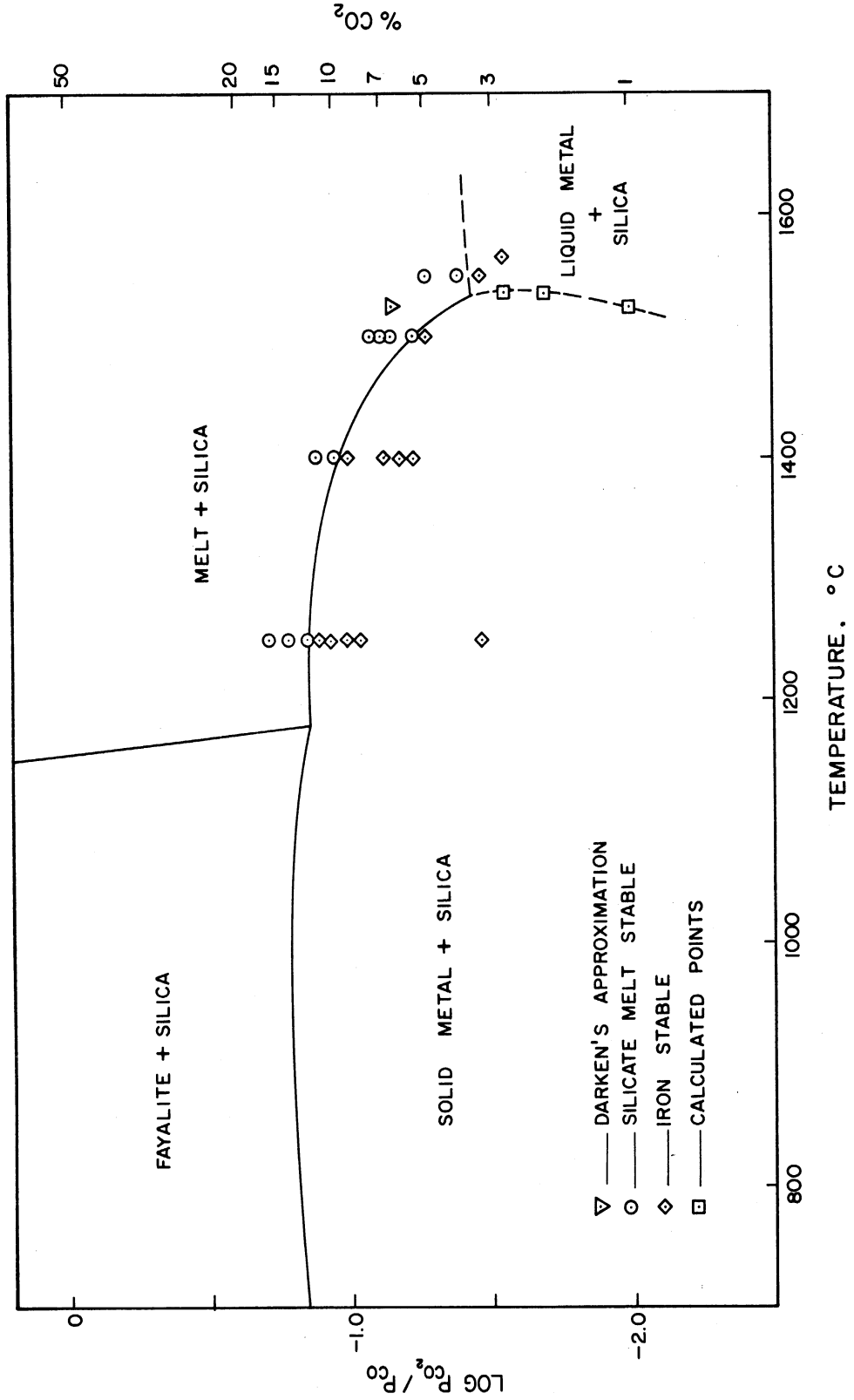

Iron, silicon, oxygen, carbon system
Silica side of the eutectic

Figure 46. Equilibrium diagram from Darken[16] modified to include present experimental results.

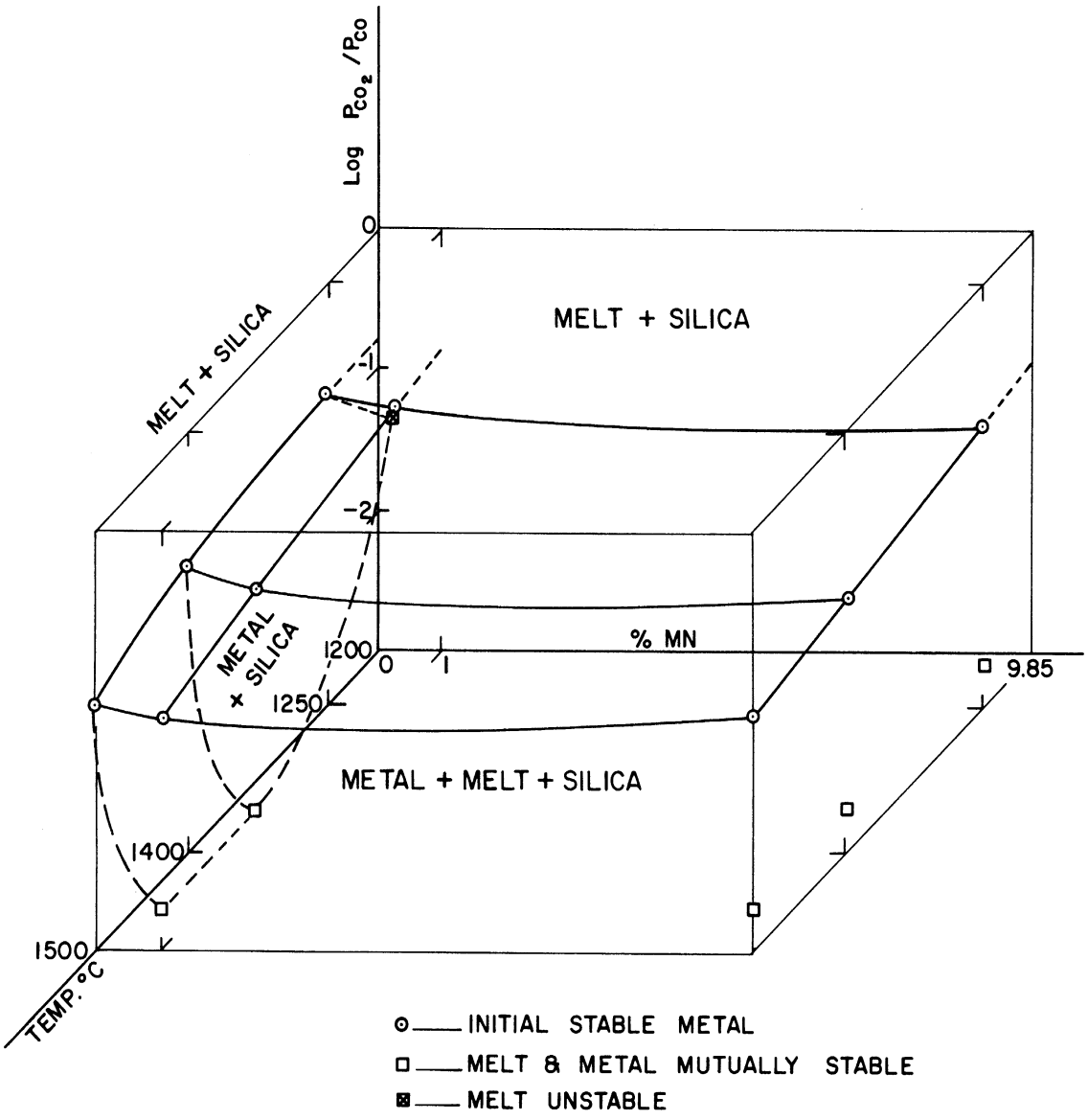

Iron, silicon, oxygen, carbon, manganese system
in the presence of excess silica

Figure 47. Equilibrium diagram from Darken[16] modified to include the effect of manganese additions.

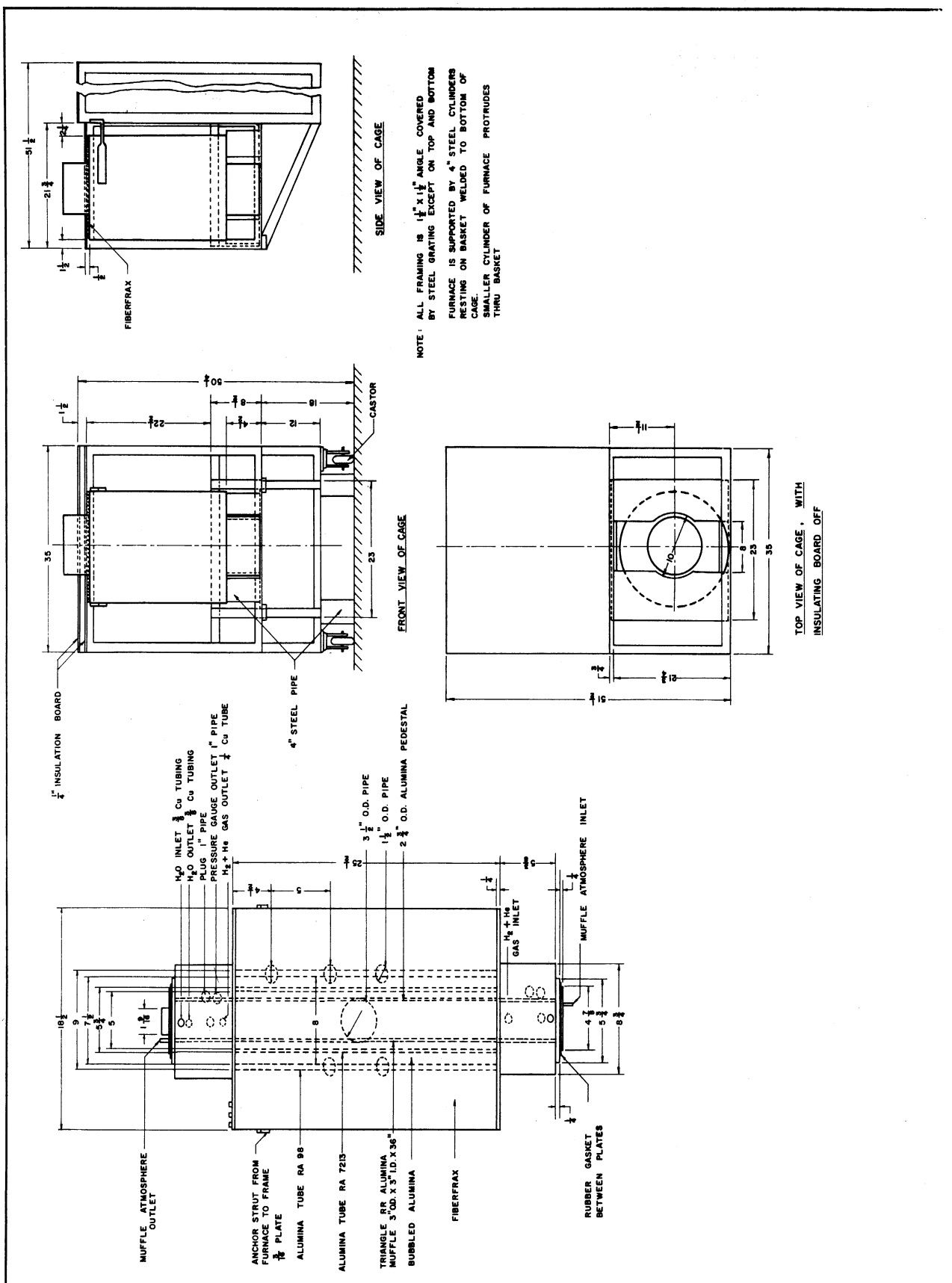

Figure 48. Detailed drawings of high-temperature furnace.

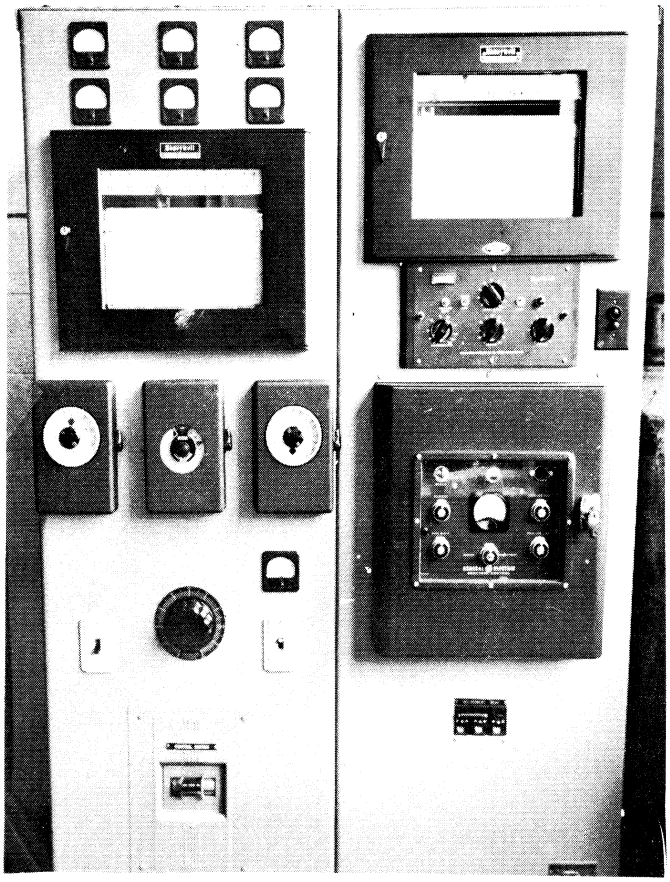

Figure 49. Photograph of high-temperature-furnace control panel.

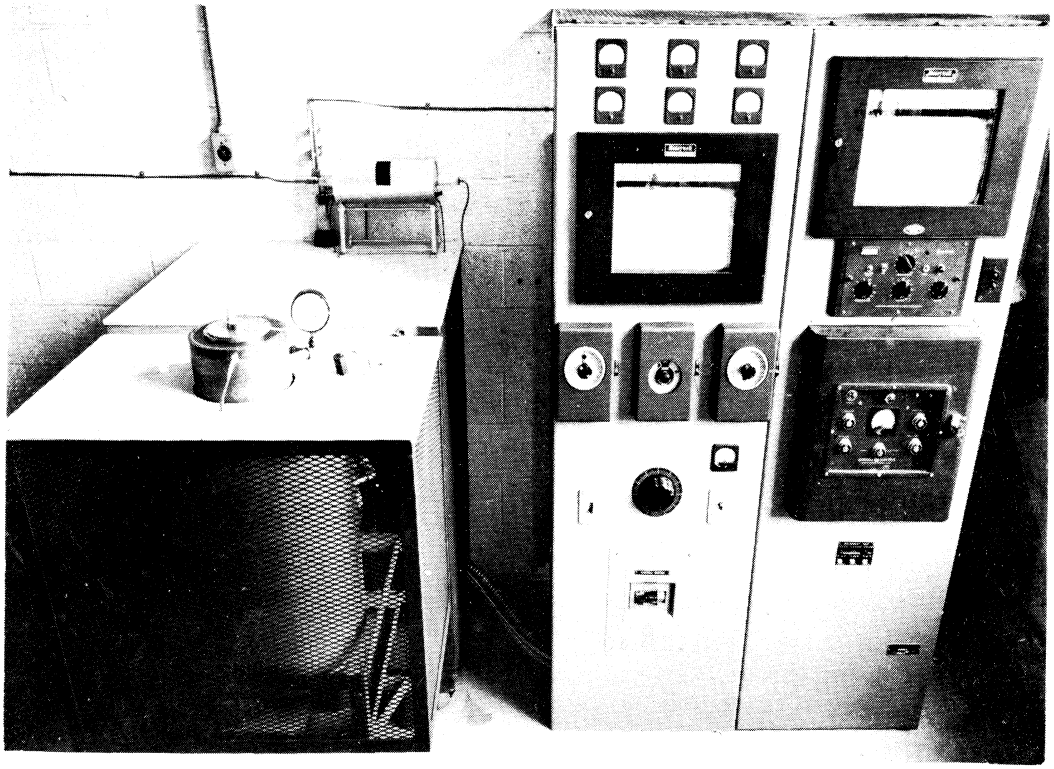

Figure 50. Photograph of high-temperature-furnace shell and control panel.

APPENDIX I

CHEMICAL COMPOSITIONS OF MINERAL PHASES

Throughout the text of this report the mineral names are used to identify all non-metallic phases. The compositions of these phases are as follows:

quartz	SiO_2 stable form to 870°C (1600°F)
cristobalite	SiO_2 stable form from 1470°C (2680°F) to 1710°C (3110°F)
tridymite	SiO_2 stable from 870°C (1600°F) to 1470°C (2680°F)
fayalite	Fe_2SiO_4
magnetite	Fe_3O_4
hematite	Fe_2O_3
liquid silicate	x(FeO) y(MnO) z(SiO_2)

The following code is used to identify the phases presented in the photomicrographs:

Code Symbol	Phase
Q	quartz
C	cristobalite
T	tridymite
F	fayalite
M	magnetite
H	hematite
I	iron
B	bakelite

APPENDIX II

HIGH TEMPERATURE FURNACE CONSTRUCTION

The equilibration phase of this experimental investigation was performed in a molybdenum resistance furnace. Figure 48 contains a detailed drawing of the construction of the furnace shell and muffle. The heat source in this furnace is three resistance coils in a controlled reducing atmosphere. Non-flammable hydrogen and helium gas mixtures are used to prevent oxidation of the molybdenum coils. The atmosphere on the coils is sealed from the internal muffle atmosphere by water-cooled silicone rubber gaskets. The muffle is a Triangle RR grade recrystallized alumina tube, 3-inch ID x 36 inches long. For extended time periods at elevated temperature with controlled atmosphere the alumina muffle is superior to a mullite tube.

The muffle atmosphere enters at the bottom and passes up the tube past the sample which rests on the alumina pedestal and plaque. This flow minimizes the problem of gas separation by thermal diffusion. As outlined in the text the temperature and atmosphere in the muffle were carefully calibrated.

The controller for this furnace is a radiation pyrometer which sights on the closed end of a mullite tube. The end of the mullite tube is in contact with the center molybdenum resistance coil. Extremely sensitive control is possible using this type of construction. The radiation pyrome-

ter thermopile sends a direct current signal to the controller. Figure 49 is a photograph of the control panel. The proportioning controller amplifies the signal and sends this voltage to the General Electric Reactrol panel. Power to the coils is varied by the throttling effect of this d-c voltage on the impedance of three saturable core reactors. As the controller calls for power the impedance of the reactors is reduced by the d-c winding around the reactors. This allows more voltage to be applied to three individual autotransformers. The autotransformers in turn raise the amperage and decrease the voltage applied to the resistance coils. Figure 50 contains a photograph of the control panel and furnace shell. The furnace and controls are designed to allow predetermined heating rates, soak times and cooling rates in addition to extended equilibration investigations. The left side of the control panel contains the auxiliary equipment for the furnace as follows:

1. Ammeter and voltmeter for each coil
2. Strip chart recorder for specimen temperature
3. Upscale interrupter, soak timer, downscale interrupter
4. Powerstat for chip furnace
5. Ammeter and control for vacuum pump.

Due to line voltage variation temperature control at the set point will vary from ± 0° to ± 2°C.

APPENDIX III

CALCULATION OF UNIVARIANT EQUILIBRIUM SOLID METAL, LIQUID METAL, SILICA, GAS

If the effect of solid silica is neglected, due to its extremely low solubility, the position of this univariant curve may be approximately calculated from the following reaction:

$$CO_2 + \underline{C} \rightarrow 2\ CO$$

$\Delta H^\circ = +29{,}560$ cal/mol $\qquad \Delta S^\circ = +28.34$ cal/mol/°K

where

$$\log K = \frac{-\Delta H^\circ}{(4.575)\ (T)} + \frac{\Delta S^\circ}{4.575}$$

$$K = 407 \text{ at } 1530^\circ C$$

$$K = \frac{(a_{CO})^2}{(a_{CO_2})\ (a_{\underline{C}})} = \frac{(p_{CO})^2}{(p_{CO_2})\ (\text{wt } \% \ \underline{C})}$$

By calculating the equilibrium constant at 1530°C a wt % $\underline{C}$ can be determined for any desired gas mixture. With the wt % $\underline{C}$ in the iron known the liquidus temperature can be determined from the iron-carbon equilibrium diagram. If the liquidus temperature varies appreciably from the assumed temperature, the new temperature may be used to calculate a corrected equilibrium constant. The initial liquidus temperature may then be corrected to minimize any deviation due to equilibrium constant variation with temperature.

A sample calculation follows:

Assuming T = 1803°K

$$K = 407 \ .$$

With the atmosphere 2.0% CO_2 - 98.0% CO then

$$\text{wt \% } \underline{C} = \frac{(.98)^2}{(.02)\ (407)} = .118\% \ \underline{C} \ .$$

The results of these calculations are included in Table V.

Thermodynamic data used in these calculations were obtained from "Basic Open Hearth Steelmaking," A.I.M.E., 1951.

BIBLIOGRAPHY

1. Murton, A. E., and Gertsman, S. L., "A Literature Review of Metal Penetration," Trans. AFS, 66, 1-6 (1958).

2. Caine, J. B., "A Study of Burnt-On or Adhering Sand," Trans. AFA, 51, 647-705 (1943).

3. Dietert, H. W., Doelman, R. L., and Bennett, R. W., "Mold Atmosphere Control," Trans. AFA, 52, 1053-1077 (1944).

4. Savage, R. E., and Taylor, H. F. "Fayalite Reaction in Sand Molds Used for Making Steel Castings," Trans. AFS, 58, 564-577 (1950).

5. Giller, D. L., unpublished report, Univ. of Mich., Ann Arbor, 1955.

6. Hoar, T. P., and Atterton, D. V., "Penetration of Molten Metal into Molding Sand," J. Iron Steel Inst., 167, 141-157 (1951).

7. Atterton, D. V., "Factors Affecting the Surface Finish of Steel Castings," Foundry, 86, Nos. 1, 2 and 3, 78, 107, 92 (1958).

8. Kozakevich, P., Chatel, S., and Sage, M., "Chemie physique--Sur la tension superficielle des alliages liquides fer-carbone," Comptes Rendus, 236, 2064 (1953).

9. Halden, F. A., and Kingery, W. D., "Surface Tension at Elevated Temperatures," J. Phys. Chem., 59, No. 6, 557-559 (1955).

10. Petersson, Holger, "An Investigation of the Penetration of Steel into Molding Sand," Trans. AFS, 59, 35-55 (1951).

11. Emmons, R. C., and Bach, J., "Steel Penetration," Foundry, 83, No. 4, 3-11 (1955).

12. Bowen, N. L., and Schairer, J. F., "The System FeO-SiO_2," Amer. J. of Science, 24, 177 (1932).

13. Muan, A., "Phase Equilibria in the System FeO-Fe_2O_3-SiO_2," J. of Metals, 7, No. 9, 965-976 (1955).

14. Koerber, F., and Oelsen, W., "The Relations Between Iron Containing Manganese and Slags Consisting Almost Exclusively of Manganous Oxide and Ferrous Oxide," Mit. a.d. Kaiser-Wilhelm Inst. Eisenforsch., 14, 181-204 (1932).

15. Darken, L. S., and Gurry, R. W., "The System Iron-Oxygen, J. ACS, 67, 1398-1412 (1945).

16. Darken, L. S., "Melting Points of Iron Oxides on Silica; Phase Equilibria in the System Fe-Si-O as a Function of Gas Composition and Temperature," J. ACS, 70, 2046-2053 (1948).

17. Case, L. O., Elements of the Phase Rule, The Edwards Letter Shop, Ann Arbor, Mich., 1939.

18. Colligan, G. A., Van Vlack, L. H., and Flinn, R. A., "The Effect of Temperature and Atmosphere on Iron-Silica Interface Reaction," Trans. AFS, 66, 452-458 (1958).

19. Wells, R. G., Van Vlack, L. H., and La Londe, R., "The Effect of Ferrous Oxide on Zircon Sand at 1200°C (2192°F)," paper presented before the American Ceramic Society, Pittsburgh, Pa., April 30, 1958.

20. Van Vlack, L. H., Wells, R. G., and Pierce, W. B., "Reduction of Silica in Large Shell Molds," Trans. AFS, 66, 459-465 (1958).

UNIVERSITY OF MICHIGAN
3 9015 02841 2925